The response of two-phase hydrothermal systems to changing magmatic heat input at mid-ocean ridges

Jaewoon Choi

Thesis submitted to the faculty of the Virginia Polytechnic Institute and State University in partial fulfillment of the requirements for the degree of

Master of Science

In

Geosciences

Robert P. Lowell

John A. Hole

Esteban Gazel

April 09, 2013

Blacksburg, VA

Keywords: hydrothermal system, two-phase flow, mid-ocean ridges, magmatic heat

The response of two-phase hydrothermal systems to changing magmatic heat input at mid-ocean ridges

Jaewoon Choi

ABSTRACT

Hydrothermal processes at oceanic spreading centers are largely influenced by changing magmatic heat input. I use the NaCl-H_2O FISHES code to investigate the evolution of surface temperature and salinity as a function of time-varying heat flux at the base of a two-phase, vapor-brine hydrothermal system. I consider a two-dimensional rectangular box that is 1.5 km deep and 4 km long with homogeneous permeability of 10^{-13} m^2. Temperature and pressure at top boundary correspond to seafloor conditions of 10°C, 25MPa respectively. Impermeable, insulated conditions are imposed on the left and right hand boundaries. To simulate time-varying heat flux from a sub-axial magma chamber of 500 m long half-width, I consider a variety of basal boundary conditions: (1) a constant heat flux with an value of 130 W/m^2; (2) a sinusoidal heat flux with a period of 6 years and an amplitude ranging between 100 and 50 W/m^2; (3) step, random, and exponential heat fluxes ranging between 200 and 15 W/m^2; and (4) an analytical function of temporally decaying heat flux resulting from a simulated cooling, crystallizing magmatic sill. As a result of the investigation I find: (1) changes in bottom temperature and salinity closely follow the temporal variations in magmatic heat inputs; (2) the surface temperature response is severely damped and high frequency variations in heat flow are not detected; (3) in regions where phase separation of vapor and brine occurs, surface salinity variations may be recorded in response to changing conditions at depth, but these are smaller in amplitude.

DEDICATION

This work is dedicated to my wife Eunju, daughters Ahin and Jeein.

ACKNOWLEDGEMENTS

I would like to thank my advisor, Dr. Robert P. Lowell, for his support and insights throughout this study. Also I would like to thank my committee members, Dr. John A. Hole and Dr. Esteban Gazel for their guidance and suggestions on this thesis. During the two years, I have received a lot of helps from colleagues, faculty and staff in the Department of Geosciences at Virginia Tech. I must express my gratefulness to all of them.

Finally, I wouldn't be here without supports from my company Korea Gas Corporation (KOGAS). This research was supported in part by NSF Grant OCE 0926418 to R.P.L.

TABLE OF CONTENTS

LIST OF TABLES

LIST OF FIGURES

CHAPTER 1: INTRODUCTION

1.1 General background on seafloor hydrothermal systems

Hydrothermal systems at mid-ocean ridges have been studied for more than three decades since black smokers were first discovered on the East Pacific Rise in 1979 [*Spiess et al.,* 1980*; Macdonald et al*., 1980]. As a combination of the words of hydro and thermos, hydrothermal implies a linkage between water and heat. Thus hydrothermal systems consist of a heat source and a fluid circulation within the Earth's crust. At mid-ocean ridges, the heat for high-temperature hydrothermal circulation primarily comes from underlying magma bodies, and the circulating fluid is mainly seawater with minor additions of magmatic volatiles such as hydrogen, carbon dioxide, and methane [*Welhan,* 1988; *Kelly,* 1996; *Kelly et al*., 2002].

Figure 1.1 shows a conceptual model of buoyancy-driven hydrothermal circulation at a mid-ocean ridge. As cold seawater enters permeable crustal rocks and descends to near the top of the sub-axial magma chamber, heat transfer from the magma chamber body increases the fluid temperature to more than 400^{o}C. The density of fluid decreases as temperature increases, and the fluid ascends by thermal buoyancy toward the sea floor through zones of highly permeable crustal rocks, where it exits through discrete vent structures. During the circulation, sea water reacts chemically with oceanic crust. As a result, hydrothermal fluid becomes enriched in Ca, Si, and metals such as Fe, Mn, Cu, Zn and becomes depleted in Mg and SO_4 [*e.g., Von Damm et al.,* 1985; *Von Damm*, 1995]. Table 1.1 shows the differences of the chemical compositions of fluids at mid-ocean ridges compared to seawater. When the hot metal-rich hydrothermal fluid enters the ocean and mixes with cold seawater, precipitation causes a black appearance to the discharging fluid, leading to the term "black smokers" [*Haymon,* 1983; *Tivey and Delaney,* 1986]. In

addition, magmatic volatiles, CO_2, H_2, and CH_4, are added to the hydrothermal fluids [*Von Damm,* 1995, 2000*; Kelly et al*., 2002]. In addition to the chemical reactions, hydrothermal fluids may separate into a mixture of low salinity vapor and high salinity brine, particularly near the bottom of the system where the temperatures are highest. Evidence of this process, termed phase separation, comes primarily from the salinity (expressed as Cl concentration) of vent fluids [*e.g., Von Damm,* 2004*; Lowell et al*., 2008], which are typically either less than or greater than seawater [e.g., Table 1].

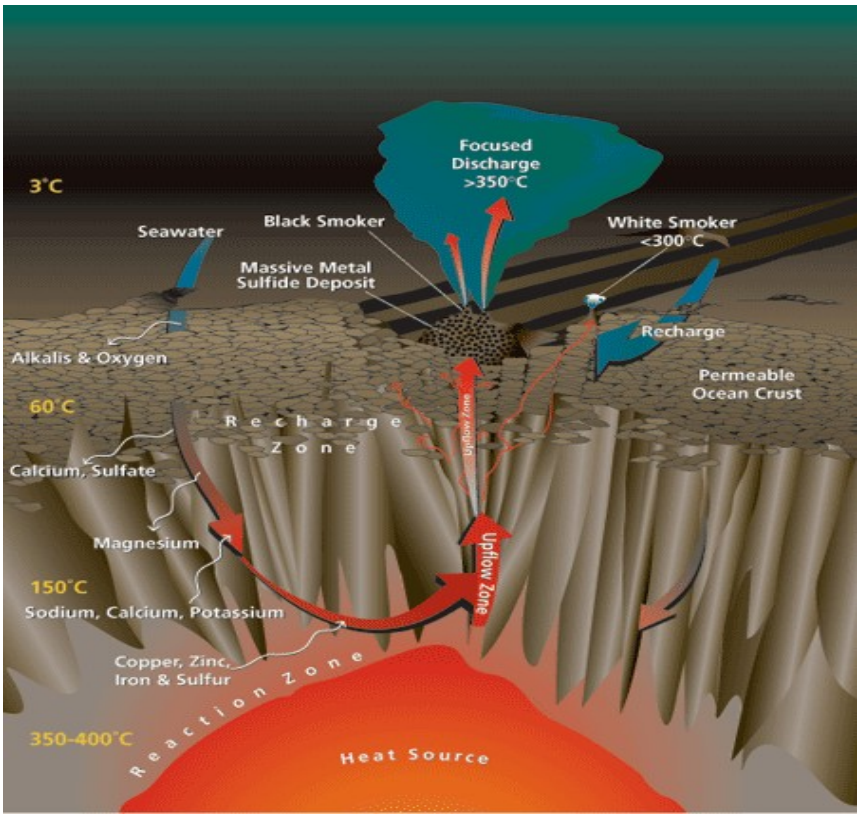

Figure 1.1 Schematic drawing of hydrothermal circulation at mid-ocean ridges [www.whoi.edu].

The linkage between the magmatic heat source and the overlying hydrothermal system at mid-ocean ridges is a subject of considerable scientific interest. As oceanic plates spread apart,

upwelling mantle beneath the ridge undergoes decompressional melting and transport to a narrow zone of crustal formation. Seismic data shows that at fast spreading ridges a zone of partially molten crust underlies a thin, mostly liquid lens of magma 10 to 100 meters thick situated between approximately 1 and 3 kilometers beneath the seafloor [*Detrick et al.,* 1987; *Sinton and Detrick*, 1992*; Sohn et al.,* 1998*; MacLeod and Yaouancq,* 2000; *Kelley et al.,* 2002; *Tolstoy et al*., 2008]. Replenishment of the magma lens, commonly called the AMC (axial magma chamber) may result in diking events and magmatic eruptions [*Germanovich et al.,* 2011]. Heat transfer from this convecting, crystallizing, replenished AMC by conduction across a thin impermeable boundary layer that lies just above the AMC drives the hydrothermal system [*e.g., Liu and Lowell,* 2009]. A key question concerns the response of the hydrothermal system to changes in magmatic heat input.

Table 1.1 Compositions of fluids venting from different settings [*from Tivey, 2007 with permission from The Oceanography Society*].

	Mid-Ocean Ridge	Back-Arc	Rainbow	Lost City	Sediment-Hosted	Seawater
T (°C)	≤ 405	278–334	365	≤ 91	100–315	2
pH (25°C)	2.8–4.5	< 1–5.0	2.8	10–11	5.1–5.9	8
Cl, mmol/kg	30.5–1245	255–790	750	548	412–668	545
Na, mmol/kg	10.6–983	210–590	553	479–485	315–560	464
Ca, mmol/kg	4.02–109	6.5–89	67	< 30	160–257	10.2
K, mmol/kg	-1.17–58.7	10.5–79	20	-	13.5–49.2	10.1
Ba, µmol/kg	1.64–18.6	5.9–100	> 67	-	> 12	0.14
H_2S, mmol/kg	0–19.5	1.3–13.1	1	< 0.064	1.10–5.98	-
H_2, mmol/kg	0.0005–38	0.035–0.5	13	< 1–15	-	-
CO_2, mmol/kg	3.56–39.9	14.4–200	na	bdl	-	2.36
CH_4, mmol/kg	0.007–2.58	.005–.06	0.13–2.2	1–2	-	-
NH_3, mmol/kg	< 0.65	-	-	-	5.6–15.6	-
Fe, µmol/kg	7–18700	13–2500	24000	-	0–180	-
Mn, µmol/kg	59–3300	12–7100	2250	-	10–236	-
Cu, µmol/kg	0–150	.003–34	140	-	< 0.02–1.1	-
Zn, µmol/kg	0–780	7.6–3000	160	-	0.1–40.0	-
Pb, µmol/kg	0.183–0.1630	0.036–3.900	0.148	-	< 0.02–0.652	-
Co, µmol/kg	0.02–1.43	-	13	-	< 0.005	-
Cd, µmol/kg	0–0.910	-	0.130	-	< 0.01–0.046	-
Ni, µmol/kg	-	-	3	-	-	-
SO_4, mmol/kg	0	0	0	1–4	0	28
Mg, mmol/kg	0	0	0	< 1	0	53

1.2 Two-phase flow

At the pressure and temperature conditions encountered near the top of the AMC, seawater exists in a liquid-vapor two-phase equilibrium state. To investigate the mass, heat, and solute transport of the hydrothermal system, seawater is assumed to be equivalent to a 3.2 wt% NaCl-H_2O solution [*Bischoff and Rosenbauer,* 1984]. Figure 1.2 shows a part of the NaCl-H_2O phase diagram with isotherms plotted onto a pressure-salinity plane. The highest point of each isotherm represents a critical point for fluid of that particular P-T-X condition, and a curve through the critical points is called the critical curve. For seawater the critical point is at approximately 407^{o}C and 298 bar [*Bischoff and Rosenbauer,* 1988]. The liquid-vapor equilibrium region lies beneath an isotherm below the critical point, and the salinity of the liquid and vapor in equilibrium at a given P-T are given by a horizontal tie line that intersects the vapor and liquid boundaries of the isotherm. High salinity liquid (commonly called brine) has a high density compared to bulk density, and thus it tends to remain at depth near the top of the AMC. Low salinity vapor is buoyant and tends to rise. This process is called phase separation. As low salinity vapor mixes with non-phase separated fluid during its ascent to the seafloor, it results in a fluid venting at the seafloor that is less than seawater. If the high salinity brine mixes with a fluid and rises, the salinity of a fluid at seafloor is greater than seawater. For this reason the salinity of a vent fluid at seafloor may vary with time. A high density layer at the base of hydrothermal system may act as a barrier between the overlying hydrothermal system and the magma chamber. In addition, magmatic eruptions or diking events may cause active phase separation in regions above the AMC. Therefore, the salinity of a vent fluid at seafloor may be low shortly after such events, to be followed by a higher salinity fluid [*Butterfield et al.,* 1997].

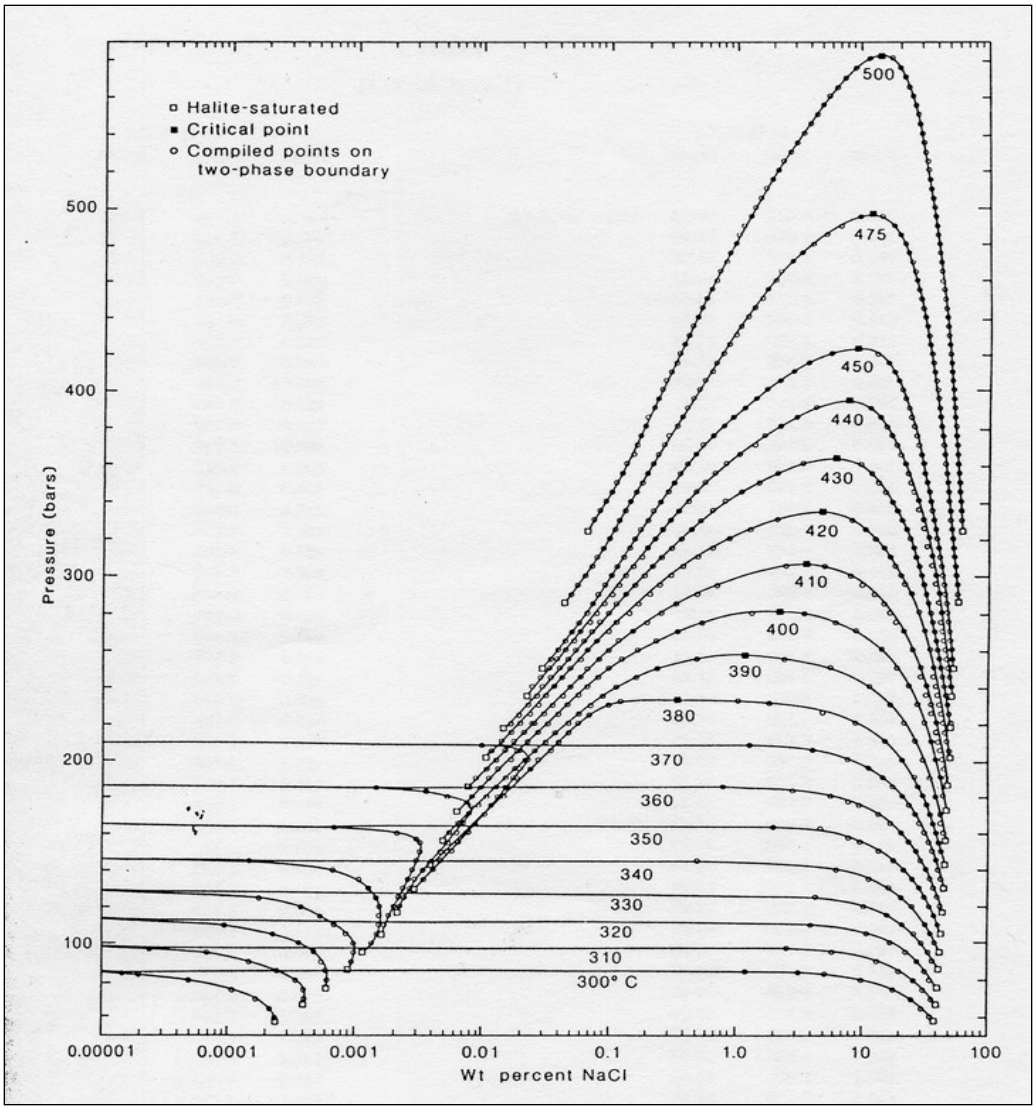

Figure 1.2 Liquid-vapor relations for the system NaCl-H_2O [*from Bischoff and Pitzer, 1989*].

1.3 Previous work on two-phase flow simulations on hydrothermal systems

The earliest models of hydrothermal systems at mid-ocean ridges have emphasized the differences between observed conductive heat flow and heat loss from lithospheric cooling models [*Bodvarsson and Lowell,* 1972; *Lister,* 1974; *Lowell,* 1975]. After the "black smokers" were found on the East Pacific Rise in 1979 [*Spiess et al.,* 1980*; Macdonald et al.,* 1980], the

need for mathematical models of high-temperature hydrothermal systems became apparent. Initially, single-phase fluid with the properties of pure water was considered as the convecting fluid for hydrothermal systems at mid-ocean ridges [*e.g., Brikowski and Norton,* 1989; *Lowell and Burnell,* 1991*; Lowell and Germanovich,* 1994; *Wilcock,* 1998]. Later boiling was considered, but the fluid was still single pure water [*Lowell and Xu,* 2000; *Coumou et al.,* 2006]. Models of two-phase flow in NaCl-H_2O fluids have only been developed recently [*Bai et al.,* 2003*; Kawada et al.,* 2004*; Lewis and Lowell,* 2004, 2009a, 2009b*; Coumou et al.,* 2008a, 2008b, 2009; *Driesner and Geiger,* 2007]. Most of these simulations assumed fixed temperature or constant heat flux at the base of hydrothermal system. The fixed temperature condition assumes that magma serves as an infinite reservoir of heat and heat transport is controlled by the vigor of the hydrothermal system, which is characterized by the Rayleigh number [*e.g., Bejan,* 1995*; Lowell and Germanovich,* 2004]. On the other hand, the thermal heat output of a constant heat flux condition is controlled by the rate at which the heat is conducted from magma body [*e.g., Lowell and Germanovich,* 1994*,* 2004; *Germanovich et al.,* 2000, 2001]. Neither of these boundary conditions is realistic because heat transfer from a convecting magma body near its liquidus will cause magma to cool and crystallize [*e.g., Cann and Srens*, 1982; *Lowell and Rona,* 1985]. The simulation of two-phase flow in NaCl-H_2O fluids with time dependent magma supply is still challenging work.

1.4 Objectives

Research on two-phase hydrothermal processes and the more broadly based magma-tectonic-hydrothermal processes have progressed independently. Models of two-phase flow described in the previous section have not incorporated magmatic heat input and its possible temporal variation directly. In contrast, *Liu and Lowell* [2009] considered heat transfer from a convecting, crystallizing, replenished magma chamber to the hydrothermal system, but two-phase hydrothermal flow was not considered and the hydrothermal system was assumed to respond instantly to changes in magmatic heat input. Therefore the need to combine the two-phase flow in NaCl-H_2O fluid hydrothermal processes with time varying magma heat supply at the base of the system is essential.

The principal objective of this study is to develop the link between time dependent magmatic heat transfer and two-phase hydrothermal circulation.

To serve as a reference, I first assume constant heat flux; then I consider sinusoidal heat flux, random heat flux, and decaying heat flux conditions. The thesis is organized as following. In chapter 2, I will review the crustal porosity and permeability and magmatic heat input as physical controls on seafloor hydrothermal activity. Chapter 3 will present the mathematical method. For the numerical method to solve the conservation equations, FISHES code [Lewis, 2007; Lewis and Lowell, 2009a, b] will be introduced. Boundary and initial conditions, the simulation method, and system geometry will be also introduced. In chapter 4, simulation results will be presented for a variety of heat flux conditions at the base of the model. Chapter 5 will discuss the implications of the results. Conclusions and recommendations for future work will be provided in Chapter 6.

CHAPTER 2: PHYSICAL CONTROLS ON SEAFLOOR HYDROTHERMAL ACTIVITY

2.1 Crustal porosity and permeability data

Porosity and permeability are important variables in hydrothermal systems, but they are difficult to characterize in the field as a result of their heterogeneity and anisotropy. Moreover, in most hydrothermal settings, including those at oceanic spreading centers, the problem is even more difficult because porosity and permeability are fracture dominated and scale dependent. Although porosity can be estimated from seismic data, permeability is not easily related to porosity. Permeability of the hydrothermal systems may also be time dependent as a result of seismic and tectonic events, dike emplacement, and mineral precipitation [*e.g., Bredehoeft et al.,* 1990]. Data from the Deep Sea Drilling Project (DSDP) and Ocean Drilling Program (ODP) determined from packer measurements provide permeability estimates to a depth of 1600m. Two sites of particular importance are Site 504B south of the Costa Rica Rift formed about 6 million years ago at a half spreading rate near 36 mm/a, and Site 1256D, which is on 15 million years old crust formed at a rate of 110 mm/a at the East Pacific Rise [*Becker,* 1989*; Fisher,* 1998*; Swift et al,* 2008*; Carlson,* 2011]. At Site 504B, the total depth is 1562.3m below seafloor, penetrating 275m of sediments, 575m of extrusive basaltic lava, a 200m transition zone, and more than 500m of the underlying layer of intrusive basaltic sheeted dikes [*Becker and Sakai,* 1989]. Two different permeability zones are found as a result of slug tests. There is a high permeability zone in the uppermost of 200m of pillow lavas where the measured permeability is approximately 10^{-14} to 10^{-13} m^2 [*Anderson and Zoback,* 1982*; Zoback and Anderson,* 1983]. There is a low permeability zone between 536.5 and 1287.5 mbsf, which corresponds to deeper pillow lavas, a transition zone, and upper sheeted dikes, where this permeability is approximately 10^{-17} m^2

[*Anderson et al.,* 1985a,b; *Becker,* 1989]. *Lowell and Germanovich* [2004] calculated the permeability ranges between 10^{-13} and 10^{-11}m^2 by using a single-pass model of the hydrothermal system constrained by typical observed values of hydrothermal temperature, hydrothermal heat output, heat uptake area and vent field area in a generic sense. *Lowell et al.* [2013], using available data from a number of actual systems, show similar ranges. The calculated bulk permeability is several orders of magnitude greater than that measured in ODP boreholes in sheeted dikes. In this paper I assumed a homogeneous permeability with value of 10^{-13} m^2.

2.1.1 Hydraulic conductivity, permeability, and relative permeability

One dimensional specific discharge q of a fluid through a porous medium is given by Darcy's Law:

$$q = -K\frac{dh}{dx} \tag{1}$$

where h is hydraulic head, and K is hydraulic conductivity, which has units of length per unit time (L/T). Similarly, the Hagen-Poiseulle law from Navier-Stokes equation for steady laminar fluid flow in a pipe is given by:

$$q = -\frac{r^2 dp}{8\mu dx} \tag{2}$$

where q is a specific discharge across the pipe, r is a radius of a pipe, μ is dynamic viscosity of the fluid, p is fluid pressure [*Sabersky et al., 1971*]. If $k = \frac{r^2}{8}$, then

$$q = -\frac{kdp}{\mu dx} = -\frac{kd(\rho gh)}{\mu dx} = -\frac{k\rho g}{\mu}\frac{dh}{dx} \tag{3}$$

The parameter k is called the permeability, which is dependent only on the material and has units of length squared($k = Cr^2$). The fluid density is ρ, and g is the acceleration due to gravity. From Darcy's law and Navier-Stokes equation the relation between hydraulic conductivity and permeability can then be expressed as:

$$K = \frac{k\rho g}{\mu} \; or \; k = \frac{K\mu}{\rho g} \tag{4}$$

In multi-phase flow in porous media, the relative permeability of a phase is a dimensionless measure of the effective permeability of that phase. Here one would expect the permeability of either fluid to be lower than that for the single fluid since it occupies only part of the pore space and may also be affected by interaction with other phases.

For two-phase flow, Darcian velocities v_v and v_l of vapor and liquid, respectively are driven by the pressure differences from the momentum conservation equations:

$$v_v = -\frac{k_v}{\mu_v}(\nabla p - \rho_v \mathrm{g}\nabla \mathrm{z}) \tag{5}$$

$$v_l = -\frac{k_l}{\mu_l}(\nabla p - \rho_l \mathrm{g}\nabla \mathrm{z}) \tag{6}$$

The subscripts *l* and *v* refer to the liquid and vapor, respectively. Relative permeabilities k_{rv} and k_{rl} are defined as:

$$k_{rv} = \frac{k_v}{k} = (1 - S^*_l)^{N_v} \tag{7}$$

$$k_{rl} = \frac{k_l}{k} = {S^*}_l^{N_l} \tag{8}$$

where k is the permeability of the porous medium in single-phase flow. The empirical parameters N_v and N_l called Corey exponents can be obtained from measured data. Normally the Corey exponents are between 2 and 4 in the oil-water system [*Dake,* 1977]. The ${S^*}_l$ from the above equations is a normalized liquid saturation defined by Corey correlation [*Corey,* 1954] as:

$${S^*}_l = \frac{S_l - S_{li}}{1 - S_{li} - S_{vi}} \tag{9}$$

where S_l is a liquid saturation. The S_{li} and S_{vi} are the irreducible residual saturations of liquid and vapor respectively. To simplify, we neglect the irreducible residual saturations and assume the parameters $N_v = 1$ and $N_l = 1$ to get a linear relationship between relative permeability and water saturation.

2.1.2 Porosity and permeability relations

Although it is generally thought that porosity and permeability are related, an exact relationship is elusive and no formulation is universally accepted. In situations in which interconnected pore space results in permeability, such permeability is termed primary permeability; whereas if permeability results from interconnected fractures the permeability is called secondary permeability.

For primary permeability, a generalized formulation of the porosity-permeability relationship can be written:

$$k = Cb^2\emptyset^n \tag{10}$$

b is an average grain size of the medium, C is a constant depending on sorting of mineral grains and $\emptyset$ a is porosity. The exponent n is typically between 2 and 3 [*Berg,* 1970*; Van Baaren,* 1979*; Nelson,* 1994; *Lowell and Rona*, 2004]. Equation (10) often fails in practice because field scale permeability is controlled by fractures.

For fracture-controlled permeability, a generalized formulation is given by equation (11):

$$k = C\frac{l^3}{L}Na^2 \tag{11}$$

where C is constant, l is mean crack aperture, L is the crack spacing, N is the number of cracks per unit area, a is crack length. As a special case of the above equation consider a set of planar parallel cracks of aperture l and spacing L. In this case the permeability can be written [*Bear,* 1972*; Turcotte and Schubert,* 1982]:

$$k = \frac{l^3}{12L} = \frac{L^2}{12}\emptyset^3 \tag{12}$$

where, assuming $l << L$, the porosity $\emptyset = l/L$. The curves of permeability and porosity show that high fracture permeability can occur in low-porosity rocks; large values of crack permeability can exist for $\emptyset \leq 1\%$ as shown in Figure 2.1.

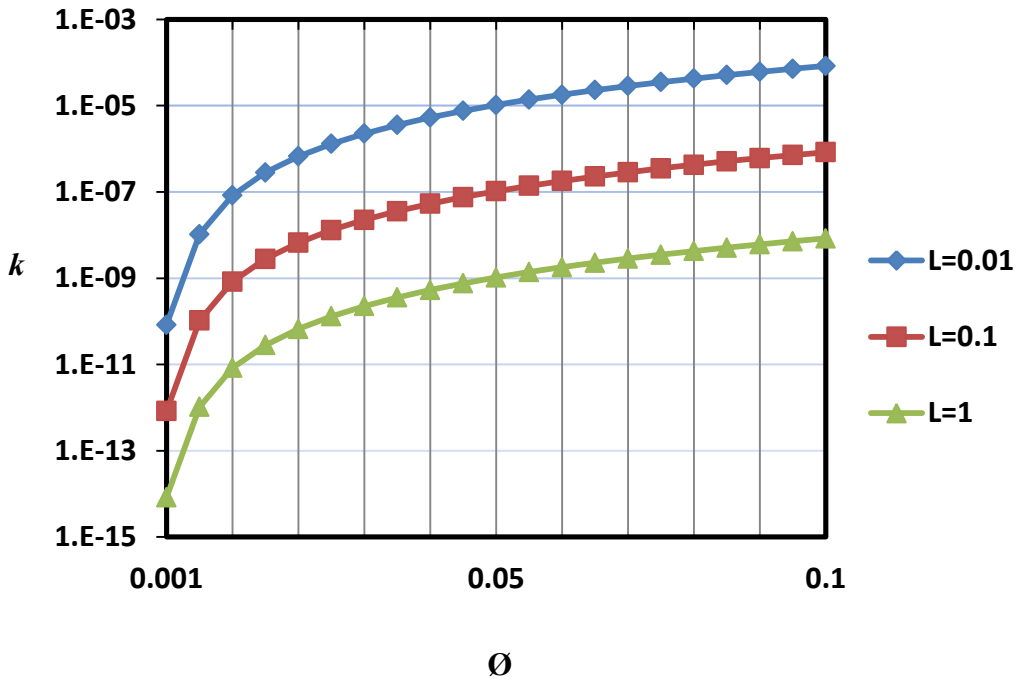

Figure 2.1 Permeability and porosity relations of fractured rocks.

2.2 Magmatic heat input

2.2.1 Magma convection

Magmatic processes such as eruption, convection, cooling and crystallization of a magma chamber significantly affect the overlying hydrothermal systems at the mid-ocean ridges. Magma convection and the resulting heat transfer to the thermal boundary layer that exists between the top of magma chamber and the base of the hydrothermal system is the primary driver of the hydrothermal system.

Compositional variations within the magma chamber result from partial melting and assimilation of overlying crust, fractional crystallization during cooling, and magma replenishment. Compositional variations are often ignored when considering basaltic magma

chambers at mid-ocean ridges. It is a reasonable first order approximation because the compositions of mid-ocean basalts are relatively homogeneous [*e.g., Batiza and Niu,* 1992; *Perfit et al.,* 1994]. *Liu and Lowell* [2009] investigated the effects of thermal convection within the magma body on heat transfer to a seafloor hydrothermal system based on an approach developed by *Huppert and Sparks* [1988] for the physics and melting of a granitic layer situated above a convecting basaltic sill. Liu and Lowell [2009] replaced the granitic layer with a parameterized hydrothermal system and assumed that heat transfer from the convecting basaltic magma chamber was transported by the hydrothermal system.

A fundamental parameter that is a measure of the strength of the convection is the dimensionless parameter called the Rayleigh number, *Ra*, which is the ratio of thermal buoyancy force to the viscous and thermal resistance. This ratio is given by

$$Ra = \frac{\alpha_m g \Delta T D^3}{a_m \nu_m} \tag{13}$$

where α_m is the coefficient of thermal expansion, g is the acceleration of gravity, $\Delta T = T_m - T_s$ is temperature difference between magma and solidus temperature of basalt, D is the thickness of a magma body, a_m is thermal diffusivity $(= \lambda_m/\rho_m c_m)$, and ν_m is the kinetic viscosity, respectively. The classical relationship between Nusselt number *Nu* and thermal Rayleigh number *Ra* is given by [*Jarvis and Peltier*,1989]:

$$Nu \sim (Ra/Ra_c)^{1/3} \tag{14}$$

where critical Rayleigh number, $Ra_c \sim 10^3$.

To investigate the response of the hydrothermal systems according to the magma chamber heat output, heat flux of the magma chamber should be studied considering magma crystallization both with and without replenishment. Heat flux from the convecting magma body is related with Nusselt number, which is the ratio of convective to conductive heat transfer across the magma body. Therefore, the heat flux F_m of the magma body can be expresses as follows

$$F_m = \frac{\lambda_m (T_m - T_s)}{D} Nu \tag{15}$$

where λ_m is thermal conductivity of magma, T_m is magma temperature, T_s is solidus temperature of the basalt, D is magma chamber thickness, respectively.

Considering the equation of Ra number of the magma convection and the relation of Nu number with Ra number, heat flux F_m transferred to the top of the magma body is given [*Turner*, 1973].

$$F_m(t) = 0.1 \rho_m c_m (\alpha_m g {a_m}^2 / \nu_m)^{1/3} (T_m(t) - T_s)^{4/3} \tag{16}$$

where ρ_m is the magma density, c_m is specific heat.

2.2.2 Magma replenishment

One of the chief results of *Liu and Lowell* [2009] was that magma replenishment is required to maintain quasi-steady hydrothermal temperature and heat output on decadal time scales. For a model of convecting magma in which crystals were assumed to settle to the floor, they found a constant velocity of the replenishment in the range of 10^{-8} ~ 10^{-7} m/s would maintain a stable hydrothermal system for decades. Their model considered a single-phase pure water hydrothermal system that responded instantaneously to changes in magmatic heat output.

In this thesis, I studied the response of two-phase hydrothermal system by using a variety of time dependent magmatic heat inputs and by incorporating a direct link to the hydrothermal system by using FISHES, which is introduced in Chapter 3.

CHAPTER 3: MATHEMATICAL METHOD

3.1 The FISHES code

FISHES (Fully Implicit Seafloor Hydrothermal Event Simulator) is a FORTRAN code that uses the finite control volume method [*Patankar*, 1980] for studying two-phase flow and phase separation in a NaCl-H_2O hydrothermal system [*Lewis*, 2007]. The *Patankar* [1980] approach takes the differential equation describing conservation of some quantity at each point in space and integrates it over a control volume, so that the resulting equation describes conservation of that same quantity over the volume. When implemented properly, the control volume method is thus guaranteed to conserve quantities such as mass, energy, and salt, both locally and globally [*Patankar*,1980].

FISHES solves the governing nonlinear partial differential equations of mass, momentum, energy, and salt in a Darcian porous medium shown below.

Mass continuity equation:

$$\frac{\partial(\emptyset\rho)}{\partial t} + \nabla \cdot (\rho_v \vec{v}_v + \rho_l \vec{v}_l) = 0 \tag{17}$$

where $\emptyset$ is the porosity, ρ is bulk density ,v is the Darcian velocity, subscripts v and l refer to the vapor and liquid phases, respectively.

Momentum conservation equation:

$$\vec{v}_v = -\frac{k k_{rv}}{\mu_v}(\nabla p - \rho_v \mathrm{g} \nabla \mathrm{z}) \tag{18}$$

$$\vec{v}_l = -\frac{kk_{rl}}{\mu_l}(\nabla p - \rho_l \mathrm{g}\nabla \mathrm{z}) \tag{19}$$

where k is permeability, k_r is the relative permeability, P is the pressure, z is the depth, μ is the dynamic viscosity and g is the gravitational acceleration.

Energy conservation equation:

$$\frac{\partial}{\partial t}[\emptyset\rho h + (1-\emptyset)\rho_r c_r \mathrm{T}] + \nabla \cdot (\rho_v h_v \vec{v}_v + \rho_l h_l \vec{v}_l) = \nabla \cdot (\lambda_m \nabla \mathrm{T}) \tag{20}$$

where h is specific enthalpy, T is the temperature, λ_m is the effective medium thermal conductivity. The subscript r refers to the rock; ρ and h without subscripts refer to bulk quantities.

Salt conservation equation:

$$\frac{\partial}{\partial t}(\emptyset\rho X) + \nabla \cdot (\rho_v \vec{v}_v X_v + \rho_l \vec{v}_l X_l) = \nabla \cdot (\emptyset\rho_v D\nabla X_v + \emptyset\rho_l D\nabla X_l) \tag{21}$$

where X is the bulk salinity and D is the salt chemical diffusivity.

In mathematical formulations using Darcy's Law to describe conservation of momentum in a porous permeable medium, an inherent assumption is that the fluid flow is laminar flow. Although Darcy's Law is empirical, it can be related to the momentum conservation equation of Navier-Stoke equations in which inertial terms are neglected and viscous flow resistance is replaced by a linear relationship. In FISHES, the relative permeabilities for the vapor and liquid phases are given by the volume saturations of vapor and liquid, respectively; and the residual saturations are assumed to be zero. FISHES discretizes the equations to produce systems of

linear algebraic equations suitable for numerical solution in a time marching scheme [*Lewis*, 2007]. The partitioning of the salt and heat between liquid and vapor phases complicates the equations of state relating pressure, temperature, and salinity (P-T-X) to fluid properties such as density and enthalpy. Hence the conservation equations must be linked to equations of state.

Lewis [2007] formulates the thermodynamic equations of state in terms of lookup tables and an interpolation scheme. The bulk densities and salinities between 300°C and 800°C used in the lookup tables come from tables presented by *Anderko and Pitzer* [1993]. For bulk density values from 0°C to 300°C, a program developed by *Archer* [1992] was used to construct the lookup tables. Specific enthalpies between 300°C and 800°C are calculated using the framework of *Tanger and Pitzer* [1989]. Enthalpies from 0°C to 300°C are used a program developed by *Archer* [1992]. Because FISHES was developed to simulate seafloor hydrothermal systems, the equations of state for the system cover the P range between 85-1000 bars, a T range between 0-800°C and a X range between 0 and 100% [*Lewis*, 2007]. The code FISHES is available online at *http://www.geophys.geos.vt.edu/rlowell/kaylal/*, and there is a user's guide with more details on the code. The code has been used previously for the simulation of two-phase hydrothermal system [*e.g., Lewis and Lowell*, 2009a, 2009b; *MacInnes* et al., 2012a, b; *Han*, 2011; *Han* et al., 2013].

3.2 System geometry, boundary and initial conditions

Seismic data show that the sub-axial magma lens (AMC) typically exists between approximately 1 and 3 kilometers beneath the seafloor [*Detrick* et al., 1987; *Canales* et al., 2006; *Singh* et al., 1999, 2006; *Van Ark* et al., 2007]. The width across-axis is typically 0.5 – 4 km [*Collier and Sinha*, 1990; Kent et al., 1990; *Singh* et al., 2006] and the vent field along-axis

spaces 1–3 km [*Gente* et al., 1986; *Kelley* et al., 2002]. Measurements of hydrothermal heat output show that it ranges between approximately 50 and 500 MW [*Lowell* and *Germanovich*, 2004; *Ramondenc* et al, 2006; *Baker*, 2007].

To investigate the evolution of surface temperature and salinity as a function of time-varying heat flux at the base of the hydrothermal system with FISHES, I considered a two-dimensional rectangular box that is 1.5 km deep and 4 km long with homogeneous permeability of 10^{-13} m^2 [Figure 3.1]. For simplicity, and to save computation time, a half-model in the lateral dimension are used as shown by the vertical dashed line in Figure 3.1. A total of 4800 elements and 4941 nodes are implemented such that each element is 25 m x 25 m.

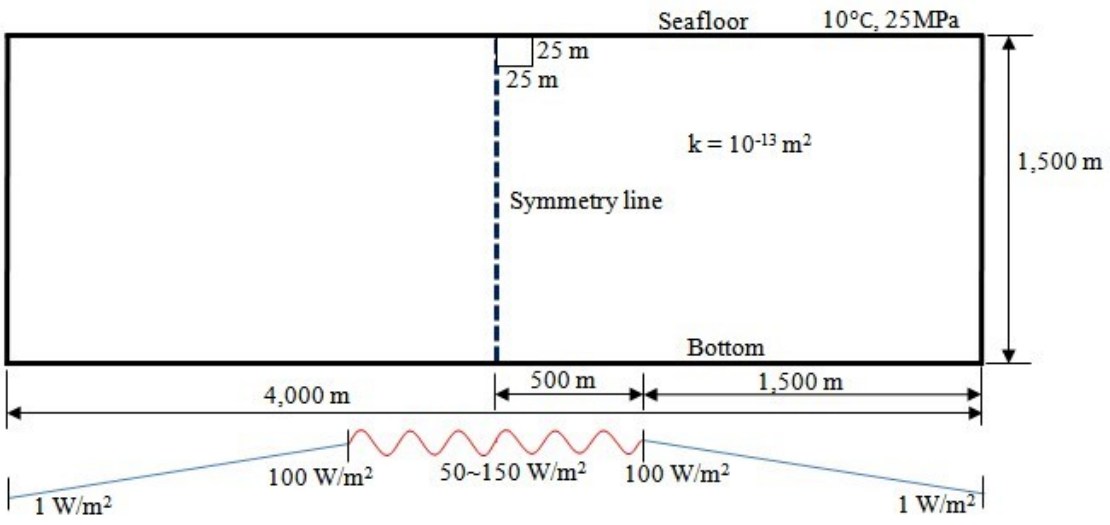

Figure 3.1 Geometry and heat flux.

Temperature and pressure at top boundary correspond to nominal seafloor conditions of 10°C, 25MPa respectively. Upstream conditions are applied at the top so temperature and salinity of fluids exiting the surface are set equal to that at one cell below the top boundary. Fluids entering

the top of the system are given seawater salinity and surface temperature conditions. Impermeable, insulated conditions are imposed on the left and right hand boundaries. The bottom boundary is also impermeable.

To simulate time-varying heat flux from the AMC, I considered a variety of basal boundary conditions: (1) a sinusoidal heat flux with a period of 6 years and an amplitude ranging between 150 and 50 W/m^2; (2) step function, random function, and exponential function between 200 and 15 W/m^2; and (3) an analytical function of temporally decaying heat flux resulting from a simulated cooling, crystallizing magmatic sill. To represent the AMC, I assumed a high heat flux region of 500 m in length to represent the approximate half-width of the magma chamber [Figure 3.1].

Initially, I assume the temperature increases linearly with depth from 10°C at the top until it matches the temperature distribution along the bottom boundary. The bottom temperature is 450°C along a region of 500m in length to simulate the AMC and decreases linearly to 300°C to the right hand edge of the box. The pressure is 25 MPa at the top and initially I assume it increases hydrostatically to the bottom. Initially, a seawater salinity of 3.2 wt% was imposed throughout the model region.

3.3 Simulation method

I used PICKUP command of the FISHES program. With this feature, the last output from a previous simulation is used as a starting input for the next simulation. For details see the user's manual at *http://www.geophys.geos.vt.edu/rlowell/kaylal/.* First, the model was run by using above initial conditions with time dependent heat flux input as a bottom boundary condition. The bottom boundary condition was a sinusoidal function of $50+25 \sin \omega t$ which has single-phase

fluids. The period of the function was about 6 years. To apply to the various time dependent heat flux of two-phase flow, it was picked up at 150 years of the simulation time. The picked temperatures of a plume at seafloor and bottom of the system are 311°C and 383°C, respectively. Second, the initial conditions of the next simulation were used from the data of the picked temperatures, pressures and salinities. The boundary conditions of the simulations of the second step were various time dependent heat flux conditions as shown in chapter 4.

CHAPTER 4: RESULTS

Temperatures and salinities of fluid discharge from a hydrothermal system are important parameters for understanding the evolution and state of the system. Convection, crystallization, and replenishment of the underlying magmatic system influence the overlying hydrothermal system by providing a time-varying heat flux. As temperatures and salinities of the discharging fluid vary with time, they can be clues to the changing magmatic heat flux. The evolution of the hydrothermal system as a result of time-varying magmatic heat flux is investigated by showing the changes of fluid temperature and salinity at the seafloor and bottom of the system. In this chapter the results for constant heat flux, oscillatory heat flux, random heat flux, and temporally decaying heat flux basal boundary conditions are shown.

4.1 Constant heat flux

Hydrothermal heat flux from an AMC with a half-width of 500 m is assumed to be 130W/m^2, and to decrease linearly from 100 to 1 W/m^2 over the rest of the bottom boundary [Figure 3.1]. This heat flux is sufficient to induce phase separation near the base of the convection system; and the convection system results in a number of high-temperature plumes situated above the magma chamber. Figure 4.1(a) shows the circulation pattern after 50 years. The circulation pattern shows a single high-temperature plume breaking into two plumes near the surface. The maximum temperature of the plume is over 400 °C and a small region of phase separation exists in the lower left-hand corner [Figure 4.1(b)]. Broad arrows highlight the general circulation pattern. The following figures show the evolution of the temperature and salinity at the surface and at the base of the system.

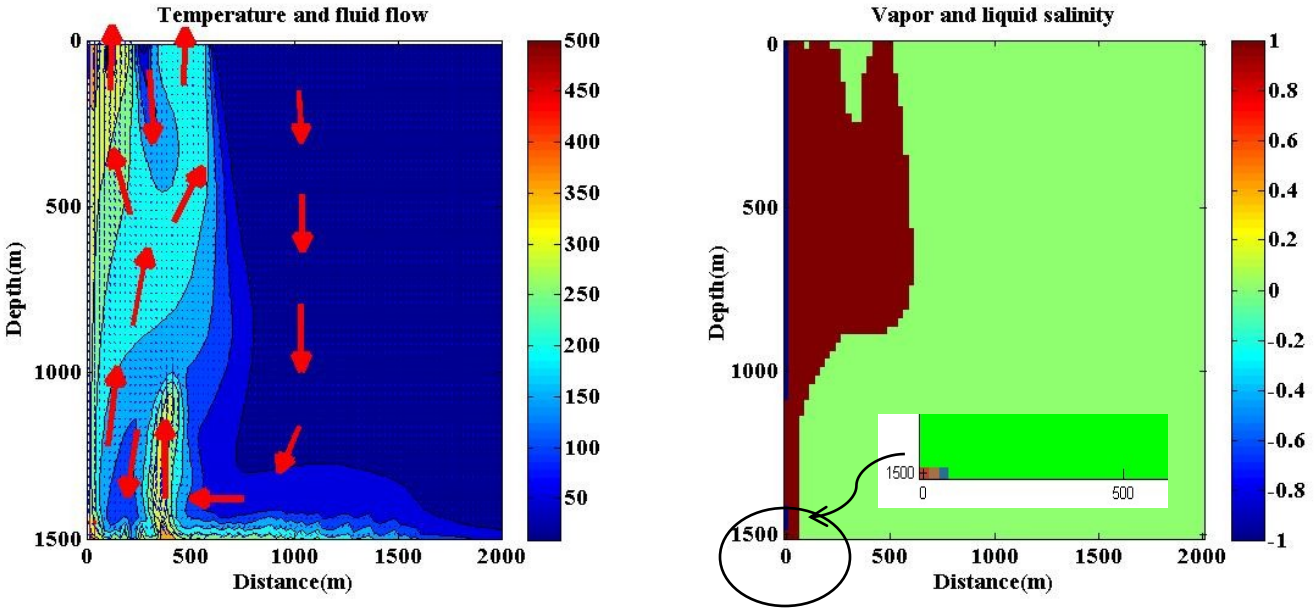

Figure 4.1 (a) Temperature distribution and schematic of fluid flow and (b) vapor and brine salinity profile at the 50 years of simulation time with constant heat flux of 130 W/m^2; In panel (b) blue color depicts salinity less than seawater; brown depicts salinity greater than seawater; green is seawater; the insert panel in (b) shows the phase separation region magnified.

Figure 4.2(a) shows the bottom temperature of the hydrothermal system as a function of time resulting from the simulation. The red line shows the temperature from the cell located in the bottom left-hand corner. The green line shows the temperature at distance of 125 m from the left-hand bottom corner. The blue line shows the temperature at distance of 325 m from the bottom left-hand corner. After 5 years of the simulation time, the temperature of the bottom left-hand corner is above 440°C, which is in the two-phase region in NaCl-H_2O phase diagram [Figure 1.2]. The temperature of the two-phase flow varies between 450°C and 500°C except for a peak after 30 years in which the temperature increases to approximately 530°C. The temperature and salinity fluctuations in space and time in this figure and subsequent ones reflect the unsteady character of high Rayleigh number convection in these simulations.

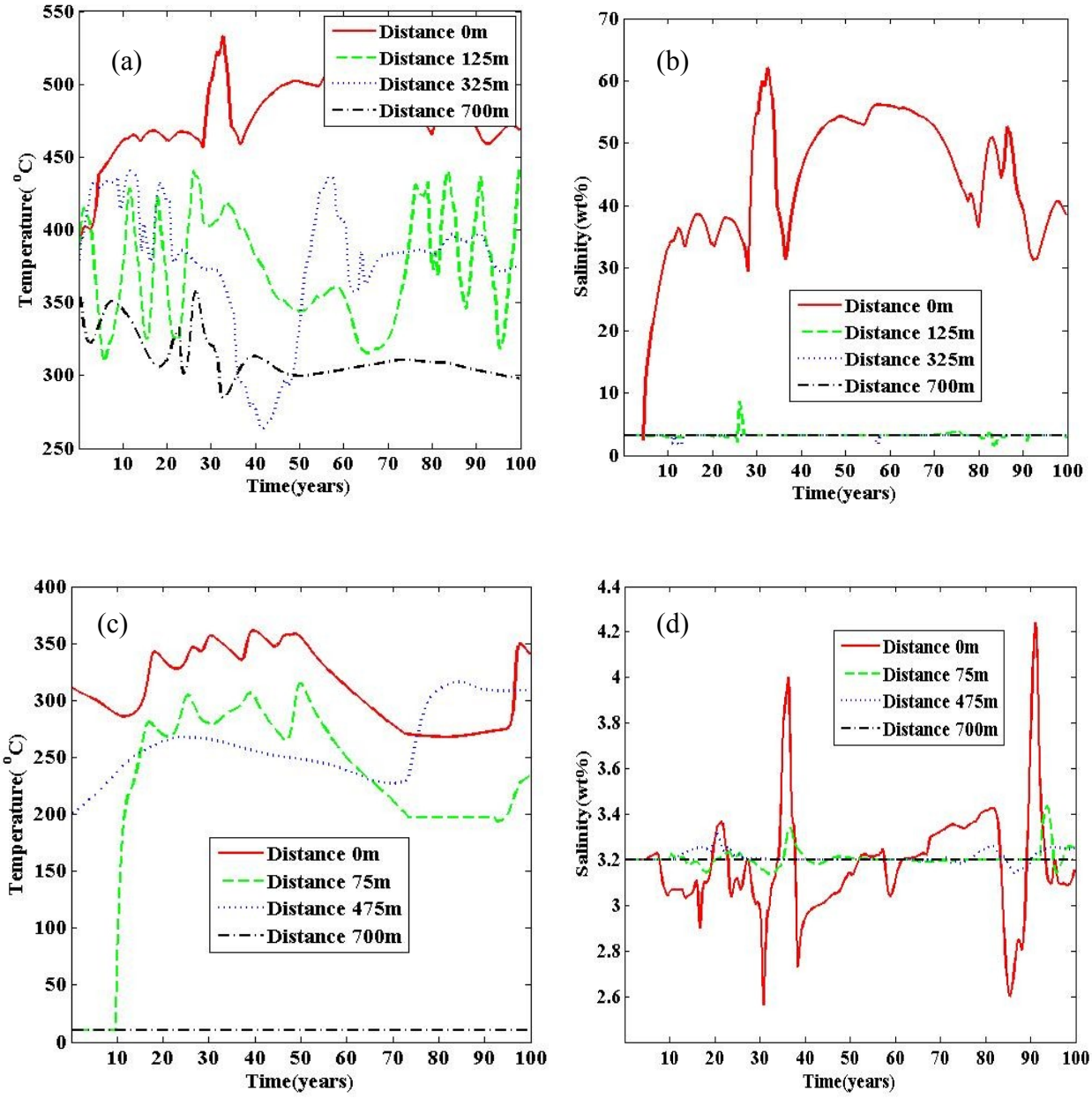

Figure 4.2 (a) Bottom temperature (b) bottom salinity (c) seafloor temperature (d) seafloor salinity for a constant heat input of 130W/m^2.

Figure 4.2(b) shows that the salinity of the bottom left-hand corner of the hydrothermal system fluctuates between 30 wt% and 60 wt%, corresponding to high salinity brine, as expected from the NaCl-H_2O phase diagram. These fluctuations are consistent with changes in salinity that result from phase separation of seawater at constant pressure as the temperature changes. The salinity far from left-hand corner is 3.2 wt% as expected for conditions corresponding to a pressure equal to 38 MPa and temperature below 440°C as shown in NaCl-H_2O phase diagram [Figure 1.2]. Figure 4.2(c) shows the seafloor temperature versus time. Conditions of phase separation observed in the bottom temperature and salinity plots [Figures 4.2 (a) and (b)] are not apparent in Figure 4.2(c). Seafloor temperatures range between 200°C and 350°C in plumes above the high-temperature bottom boundary, but at a distance of 700m, the surface temperature of 10°C indicates fluid recharge occurs to the right of the high-temperature region. Figure 4.2(d) shows the seafloor salinity at a number of distances from the left-hand boundary as a function of time. The salinity of top left-hand corner fluctuates between 2.1~3.9 wt% NaCl, which shows that both vapor- and brine-derived fluids ascend from the bottom of the system.

4.2 Oscillatory heat flux

4.2.1 Sinusoidal heat flux

For the next simulation, the heat input from the magma chamber is assumed to be a sinusoid of the form $H(t)=100+50\sin\boldsymbol{\omega}t$ W/m^2. The $\boldsymbol{\omega}$ is an angular frequency of the oscillation($\omega = \frac{2\pi}{T}$) and the period T of the oscillation is a $2\boldsymbol{\pi}$ year.

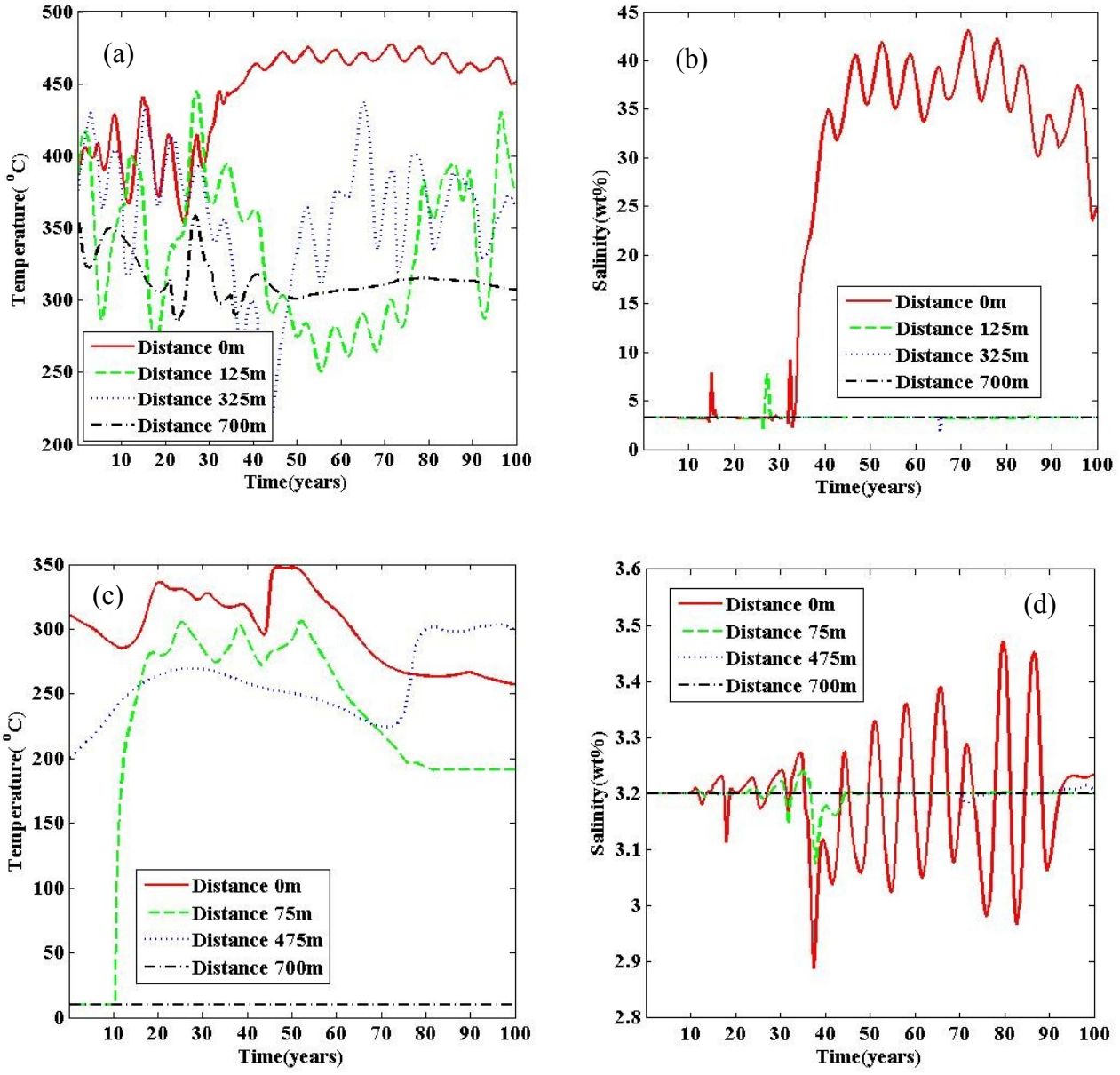

Figure 4.3 (a) Bottom temperature (b) bottom salinity (c) seafloor temperature (d) seafloor salinity for a sinusoidal heat input of $100+50\sin\boldsymbol{\omega}t$ W/m^2.

Figure 4.3(a) shows the bottom temperature of the hydrothermal system as a result of the simulation. As the period of the oscillation of the temperature is a 2π year in the region of left corner to 500m, it shows the bottom temperature of the hydrothermal system responds to the sinusoidal heat input. After 32 years of simulation time, the temperature at the left corner is above 450°C, which indicates that it is within the two-phase region. The overall temperature oscillates between 200°C and 500°C. Figure 4.3(b) shows the bottom salinity of the hydrothermal system. After 32 years of the simulation time the salinity at the left corner (distance of 0m) is greater than 30wt%, indicating that phase separation is occurring there. The salinity of the two-phase flow also shows the 2π year periodic oscillation which is the same period of heat input function. Figure 4.3(b) shows that most of the bottom of the system is in the single phase region, corresponding to basal temperature less than 440°C at P=38MPa. Figure 4.3(c) shows the seafloor temperature of the hydrothermal system as a result of the simulation. The 2π year period of oscillation from the heat input cannot be seen in the seafloor temperature. This result indicates that the seafloor temperature of the hydrothermal system does not record the periodic heat input at the base of the system, at least for an oscillation period of 6 years. The periodic character of the temperature in the ascending fluid is lost as a result of mixing along the flow path. Seafloor salinity fluctuates between 2.9~3.5 wt% NaCl, which consistent with two–phase-separated fluid ascending from the bottom of the system as shown in Figure 4.3(d). The seafloor salinity does record the periodic heat flux from the base but the amplitude of the oscillations is much smaller and it out of phase with the oscillations at the bottom.

4.2.2 Periodic rectangular heat flux

In this section, hydrothermal heat input from the magma chamber is assumed to be a periodic rectangular wave:

$$H(t) = \begin{cases} 150\ W/m^2,\ (n-1)T\ < t\ \leq \left(n-\frac{1}{2}\right)T \\ 50\ W/m^2,\quad \left(n-\frac{1}{2}\right)T < t\ \leq\ nT \end{cases},$$

where $T = 20$ years and n=1, 2, 3, 4, 5.

Figure 4.4(a) shows the bottom temperature of the hydrothermal system as a result of the simulation. The period of the temperature oscillation in the region from left corner to distance of 500 m is approximately 20 years, which is consistent with the periodic rectangular heat input wave emplaced in that region. After 4 years of simulation time, the temperature of left corner (distance 0m) is greater than 450°C, which is in the two-phase region. The overall temperature oscillates between 200°C and 500°C. Figure 4.4(b) shows that after 4 years of the simulation time the salinity at the left corner (distance 0 m) is greater than 40 wt%. The salinity of the two-phase flow approximately follows the 20 year periodic oscillation. Most area of the bottom shows the single-phase flow. Figure 4.4(c) shows seafloor temperature of the hydrothermal system. The 20 year period of oscillation from the heat input cannot be seen in the seafloor temperature. As in the case of the shorter 6-year period sinusoidal heat input, this result also indicates that the seafloor temperature does not record the 20-year periodic heat input at the base of the system. Figure 4.4(d) shows the seafloor salinity fluctuates between 2.9~3.5 wt% NaCl which indicates VDF (vapor-derived fluid) and BDF (brine-derived fluid) ascending from the bottom of the system as a result of phase separation.

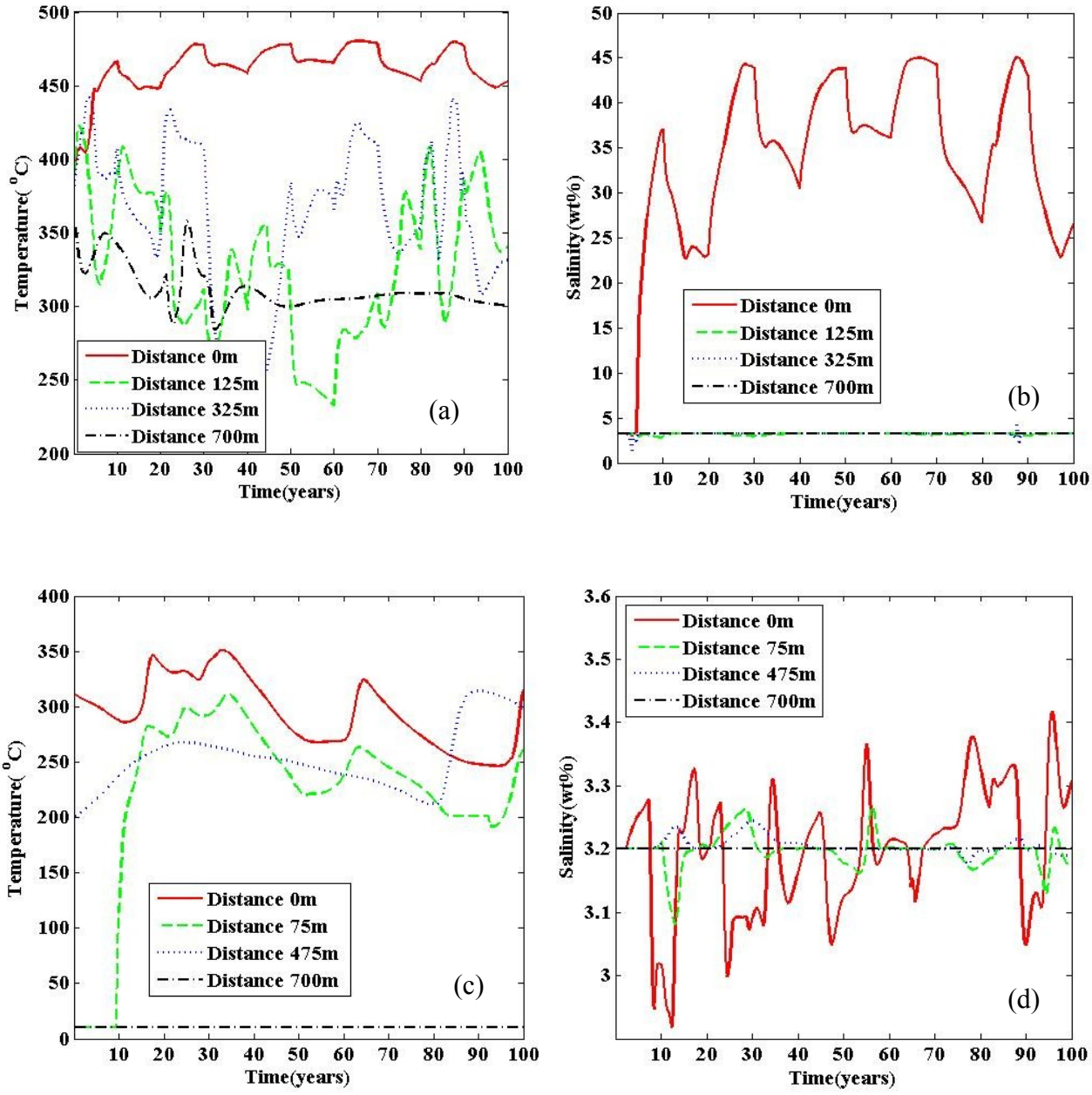

Figure 4.4 (a) Bottom temperature (b) bottom salinity (c) seafloor temperature (d) seafloor salinity for a periodic rectangular heat input.

4.3 Random heat flux

In this section hydrothermal heat input from the magma chamber is assumed to be a random function as shown Figure 4.5. The heat input is the range of 60~150 W/m^2. The random heat flow versus time is generated by MATLAB.

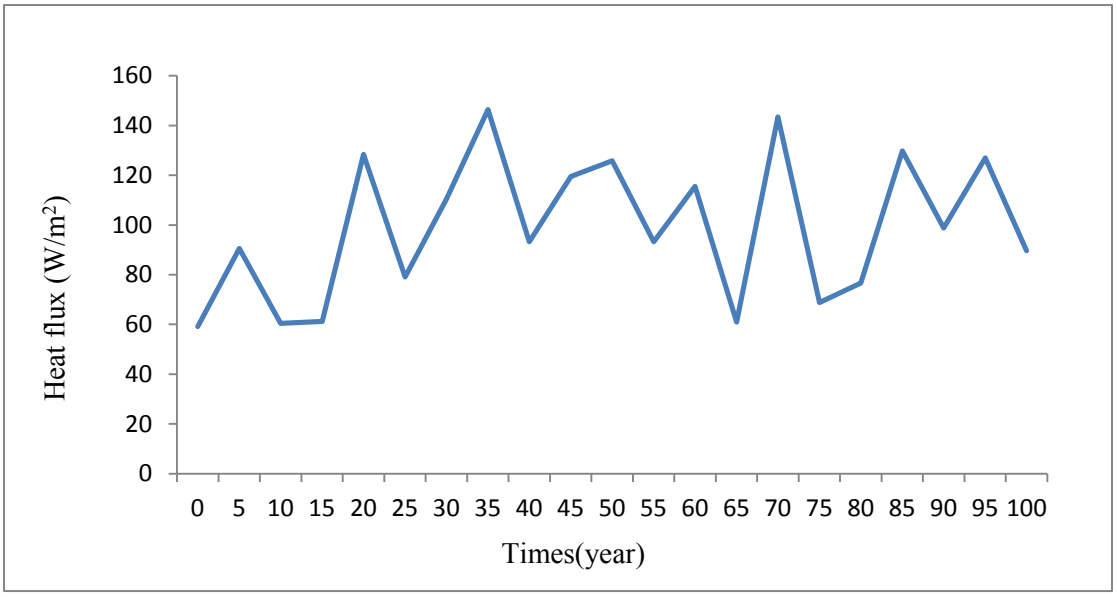

Figure 4.5 Random heat flux input as a function of time.

Figure 4.6(a) shows the bottom temperature of the hydrothermal system. After 33 years of the simulation time, the temperature at the left corner is greater than 450°C, which indicates it is within the two-phase region. The overall temperature oscillates between 200°C and 500°C. As shown in Figure 4.6(b), after 33 years of the simulation time the bottom salinity at the left corner is greater than 50 wt% which indicates phase separation occurs. Most of the bottom area of the system is in the single-phase flow regime. Figure 4.6(c) shows that phase separation that was observed in the bottom temperature and salinity is not observed at the seafloor temperature. Seafloor temperature does not record the random heat flux input. Figure 4.6(d) shows the

seafloor salinity of the hydrothermal system. The salinity fluctuates between 2.7~3.6 wt% NaCl which indicates VDF and BDF ascending from the bottom of the system. Random heat flux at the base cannot be seen clearly, however.

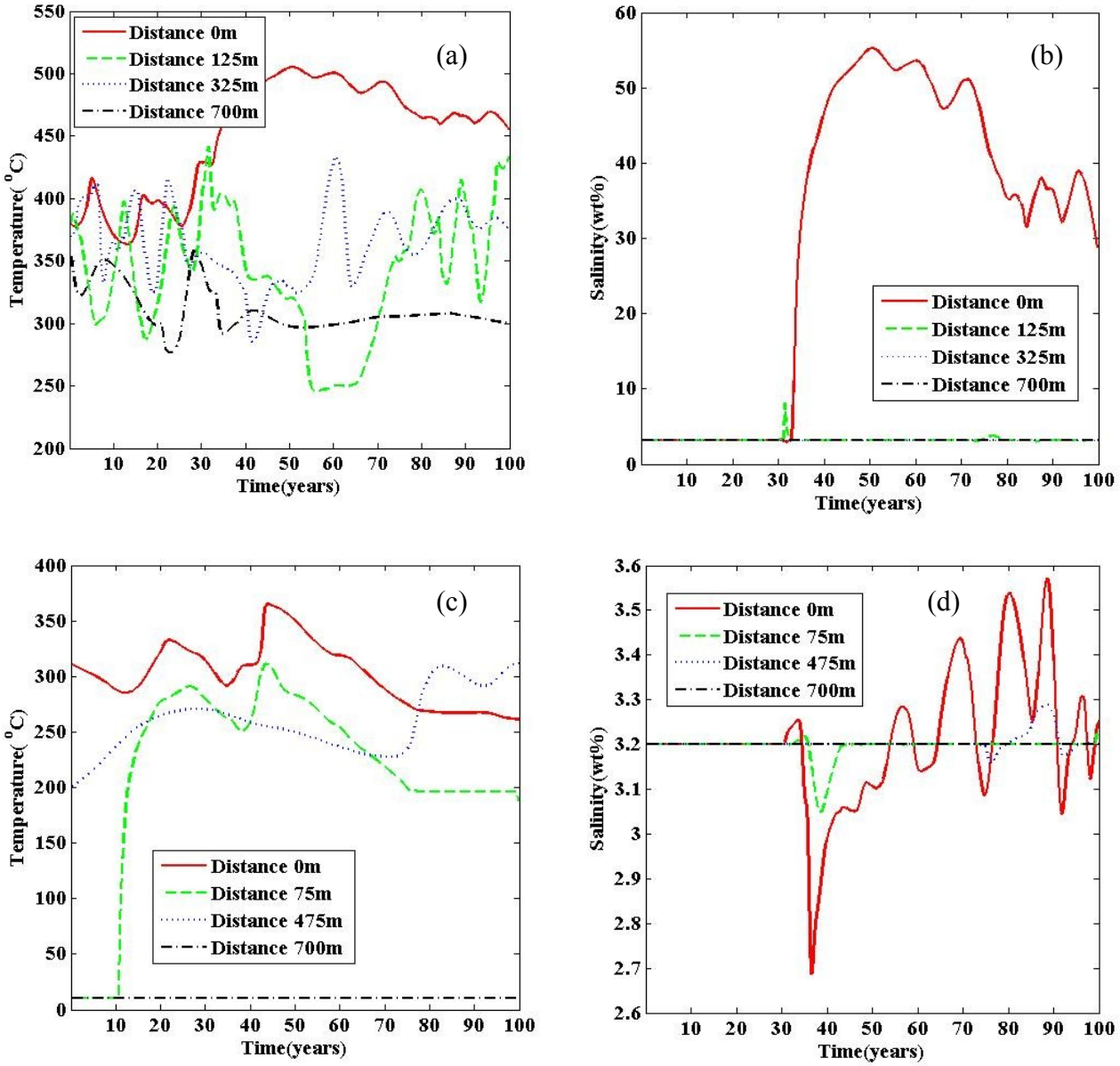

Figure 4. 6 (a) Bottom temperature (b) bottom salinity (c) seafloor temperature (d) seafloor salinity for a random heat input.

4.4 Decaying heat flux

The simulation of decaying heat from a convecting, cooling, and crystallizing magma chamber was done for the case of exponential decay, and for numerical model results from *Liu* and *Lowell* [2009] who considered a vigorously convecting sill in which crystals settled rapidly to the floor. Heat flux versus time for a convection model without replenishment, as well as for the case of crystals settling with replenishment at the velocity of 1.8×10^{-8} m/s was investigated.

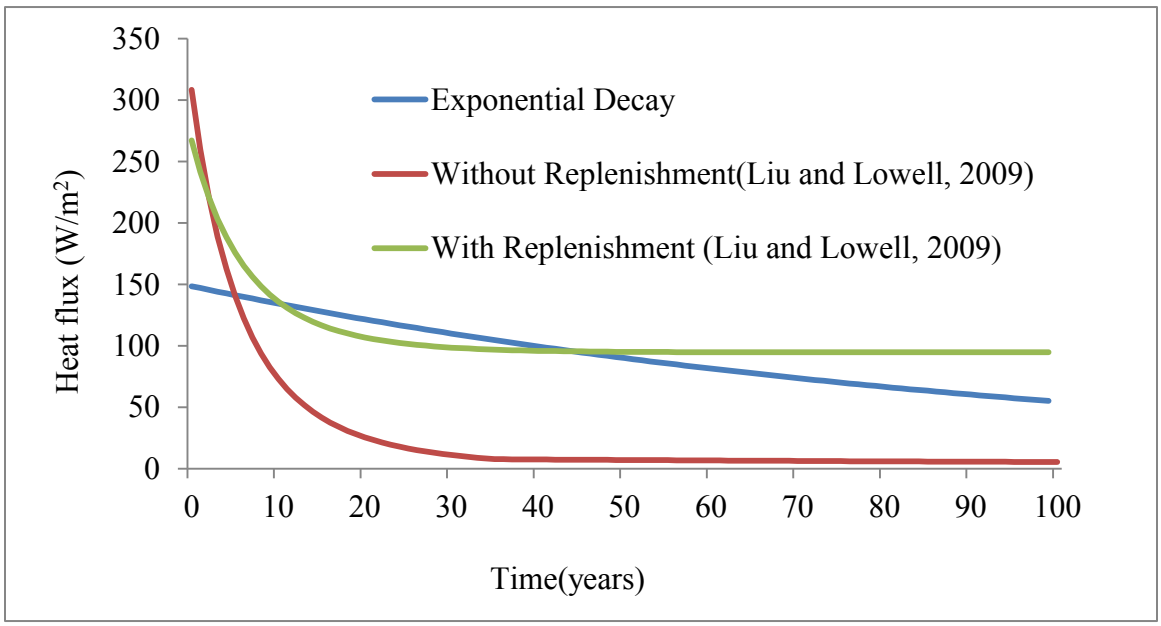

Figure 4.7 Decaying heat input.

4.4.1 Exponential decaying heat input

The hydrothermal heat input from the magma chamber is assumed to be exponential decay of the form $H(t) = H_0 e^{-\lambda t}$ W/m^2, where H_0 is an initial heat input at t = 0 and λ is a decay constant. The H_0 and λ are used as 150W/m^2 and 0.01, respectively.

Figure 4.8(a) shows the bottom temperature of the hydrothermal system as a result of the simulation. The temperatures gradually decrease as the heat input exponentially decays during simulation. After 4 years of simulation time a temperature of the left corner is greater than 450°C which indicates that phase separation is occurring. The temperature in the two-phase flow region decreases to less than 450°C after the peak in 20 years. Figure 4.8(b) shows the bottom salinity of the hydrothermal system as a result of the simulation. After 4 years of simulation time the salinity of the left corner is greater than 50 wt%, which indicates the occurrence of phase separations. The salinity of the brine rapidly decays after the peak at 20 years as does the bottom temperature. Because the basal heat flux is too low to result in phase separation after 32 years, single phase fluid circulation occurs and the fluid salinity gradually returns to that of 3.2 wt% NaCl. Figure 4.8(c) shows the seafloor temperature of the hydrothermal system. The exponential decay from the heat input is not easily observed in the seafloor temperature plot. Figure 4.8(d) shows that seafloor salinity fluctuates between 2.6~4.2 wt% NaCl which indicates VDF and BDF ascending from the bottom of the system. The final rise after 30 years indicates the ascending brine from the base. With this heat input function, the system returns to single-phase after approximately 40 years. This is shown in Figure 4.8(a) as the bottom temperature decreases below 440 °C and the basal salinity decreases to 3.2 wt% NaCl. The temperature of the venting fluid does not decrease appreciably for more than a decade, but the salinity of the vent fluid returns to the seawater value after approximately 5 years.

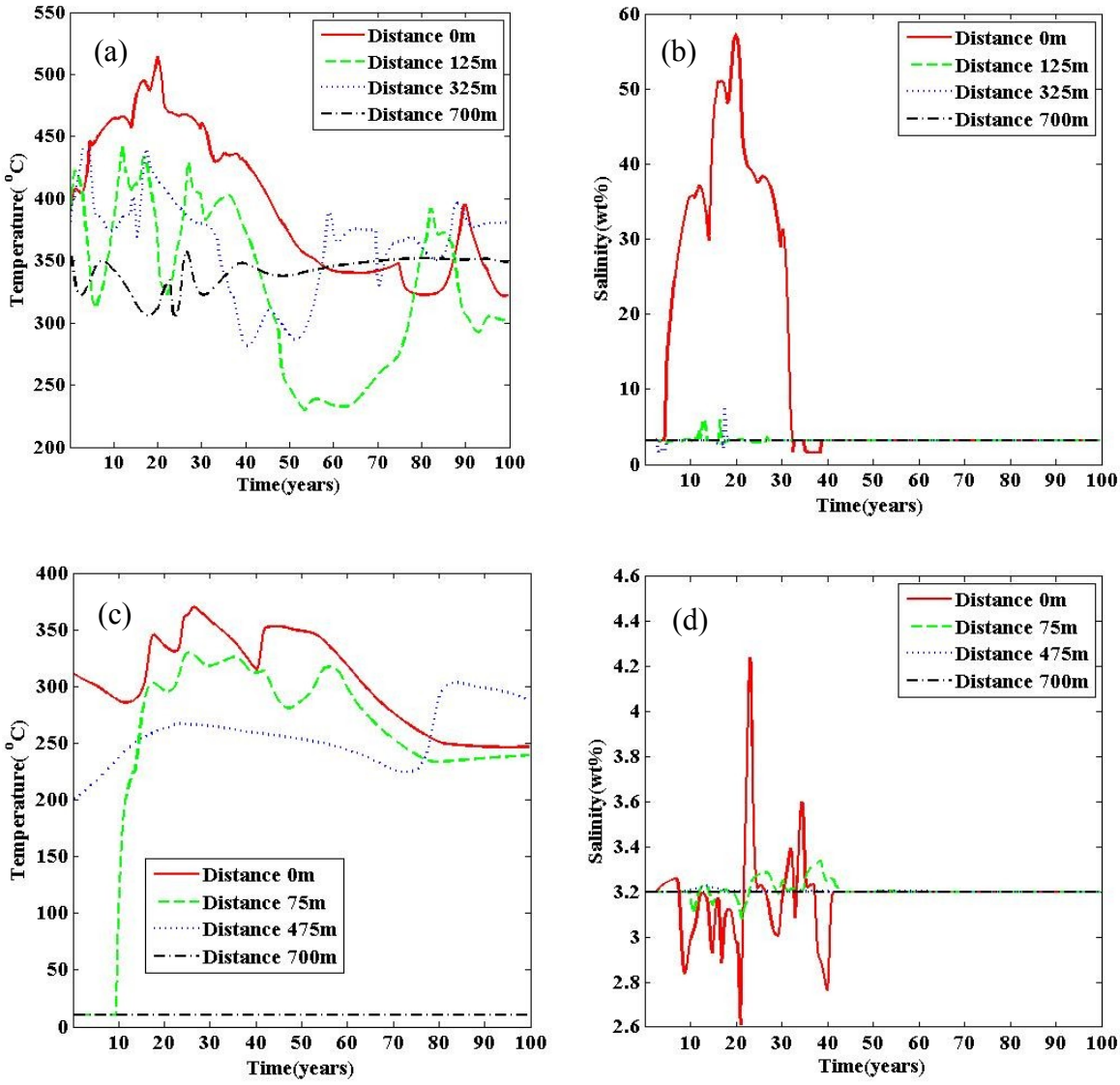

Figure 4.8 (a) Bottom temperature (b) bottom salinity (c) seafloor temperature (d) seafloor salinity for an exponentially decaying heat input.

4.4.2 Decaying heat flux: A convecting, crystallizing magma sill without replenishment

Liu and Lowell [2009] performed numerical simulations of heat output from a vigorously convecting, cooling, crystallizing magma sill in which crystals were assumed to settle rapidly to the floor. They considered cases both with and without magma replenishment. The results of these simulations are shown in Figure 4.7. Rather than link their convection model directly to FISHES simulation, I found an analytical function to fit the heat output profile and divide by the assumed area of the sill to obtain a heat flux as a function of time [Figure 4.9]. This time-dependent heat flux was then used in FISHES simulations.

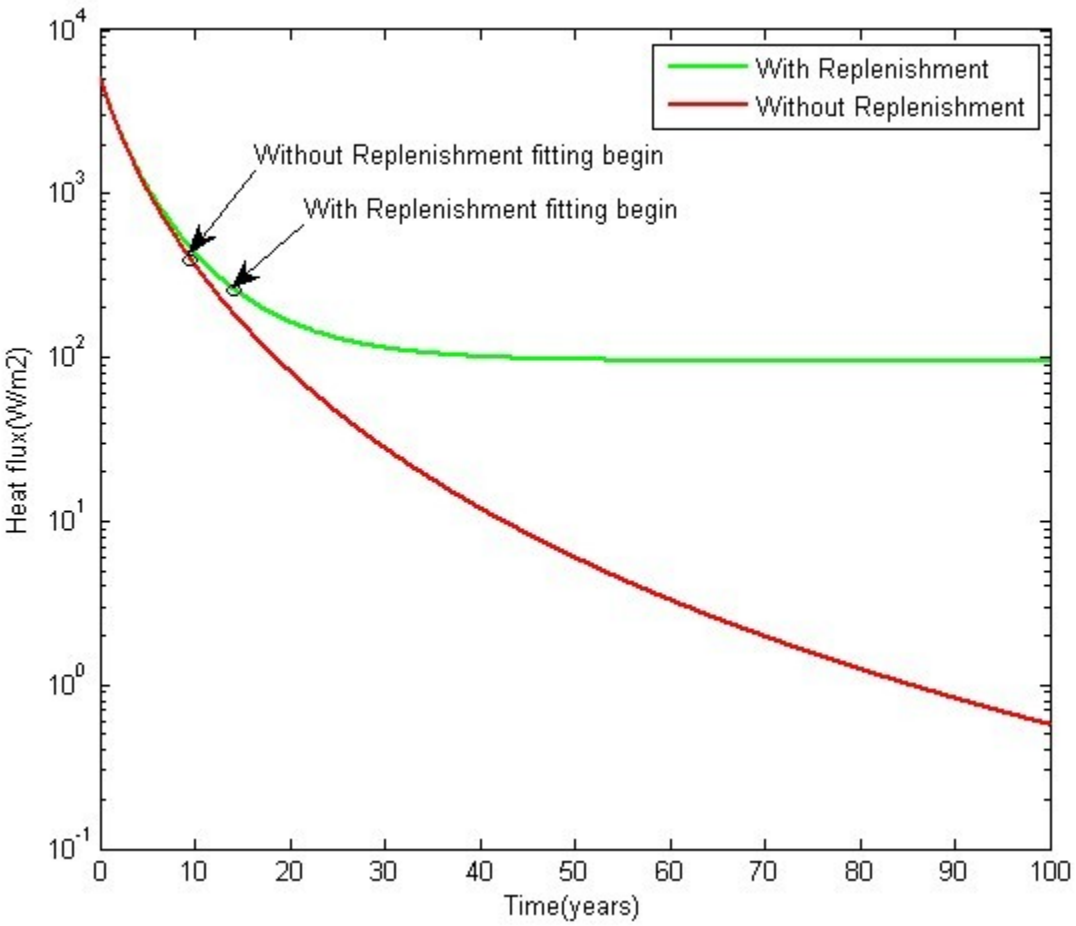

Figure 4.9 Analytical heat flux from magma chamber [*Liu and Lowell*, 2009].

Figure 4.10(a) shows the bottom temperature of the hydrothermal system without magma replenishment. The temperatures rapidly decrease as the heat input decays during simulation. The temperature of the left corner is above 450°C after 4 years of simulation time. The temperature of the two-phase flow decreases to less than 450°C after 5 years. The overall temperature decreases as the heat flux decays. Figure 4.10(b) shows that after 4 years of simulation time, the salinity of the left corner is greater than 40 wt%, but that the salinity of the brine rapidly decays after the peak at 5 years. The single-phase fluid circulation then occurs and the fluid salinity returns to 3.2 wt% NaCl after 20 years. Figure 4.10(c) shows the seafloor temperature of the hydrothermal system. The temperature decay lags far behind the decaying heat input is not easily observed in the seafloor temperature plot. Figure 10(d) shows that seafloor salinity fluctuates between 2.8~3.9 wt% NaCl which indicates the mixing between phase separated fluid and seawater as the fluid ascends. The fluctuations of salinity between 2.8 wt% and 3.7 wt% are damped in amplitude relative to the bottom salinity which varies between 0.6 wt% and 43 wt%. The sharp rise of the seafloor salinity after 20 years corresponds to the last parcel of brine rising from the base. It shows the fluid takes time to rise through the system for less than a decade.

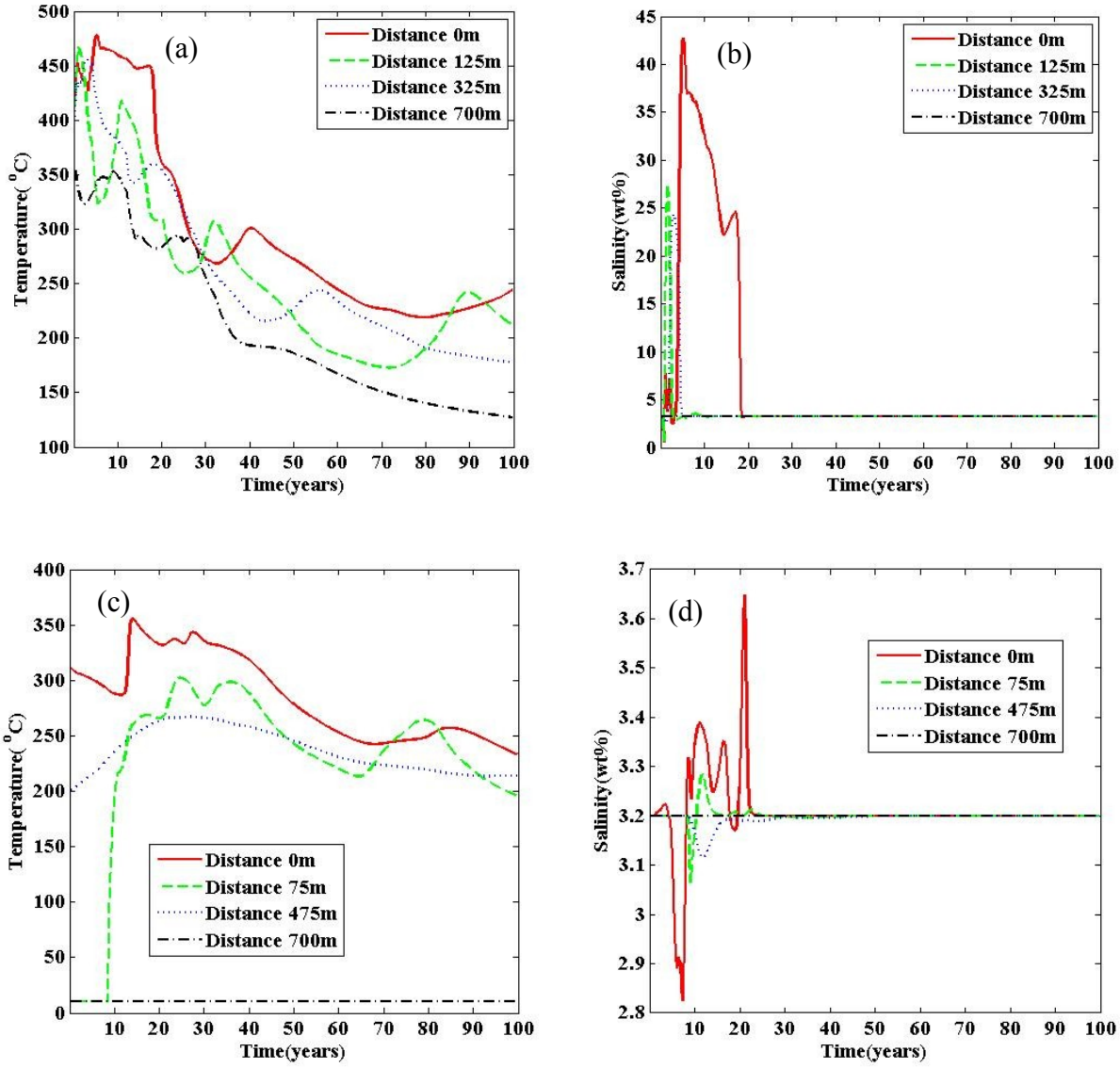

Figure 4.10 (a) Bottom temperature (b) bottom salinity (c) seafloor temperature (d) seafloor salinity for a heat input crystals settling without replenishment.

4.4.3 Decaying heat flux: A convecting, crystallizing magma sill with replenishment

Finally, the effect of magma replenishment on the response of the two-phase hydrothermal system is considered. The heat flux input is found by fitting the results of the numerical solution from *Liu and Lowell* in 2009 [Figure 4.9].

Figure 4.11(a) shows the bottom temperature of the hydrothermal system. After 3 years of simulation time, the temperature of the left corner is above 450°C which indicates that is within the two-phase region. The temperature of the two-phase flow decreases beneath 450°C after the peak in 5 years. The temperature rebounds after 10 years and shows approximately constant temperature until 80 years. The overall temperatures are the range between 250°C and 470°C. After 5 years of simulation time, the bottom salinity of the left corner is greater than 50 wt% as shown in Figure 4.11(b). The salinity of the brine decreases after the peak at 5 years and increases after 12 years as does the bottom temperature. The salinity decreases after 80 years because the heat flux input from the replenished magma is not large enough to make phase separation continuously. Figure 4.11(c) shows the seafloor temperature of the system. The decay and replenishment from the heat input is not detected at the seafloor. Seafloor salinity fluctuates between 2.6~4.0 wt% NaCl which consistent with phase-separated fluid ascending from the bottom of the system as shown in Figure 4.11(d). This pattern is similar as constant heat flux case.

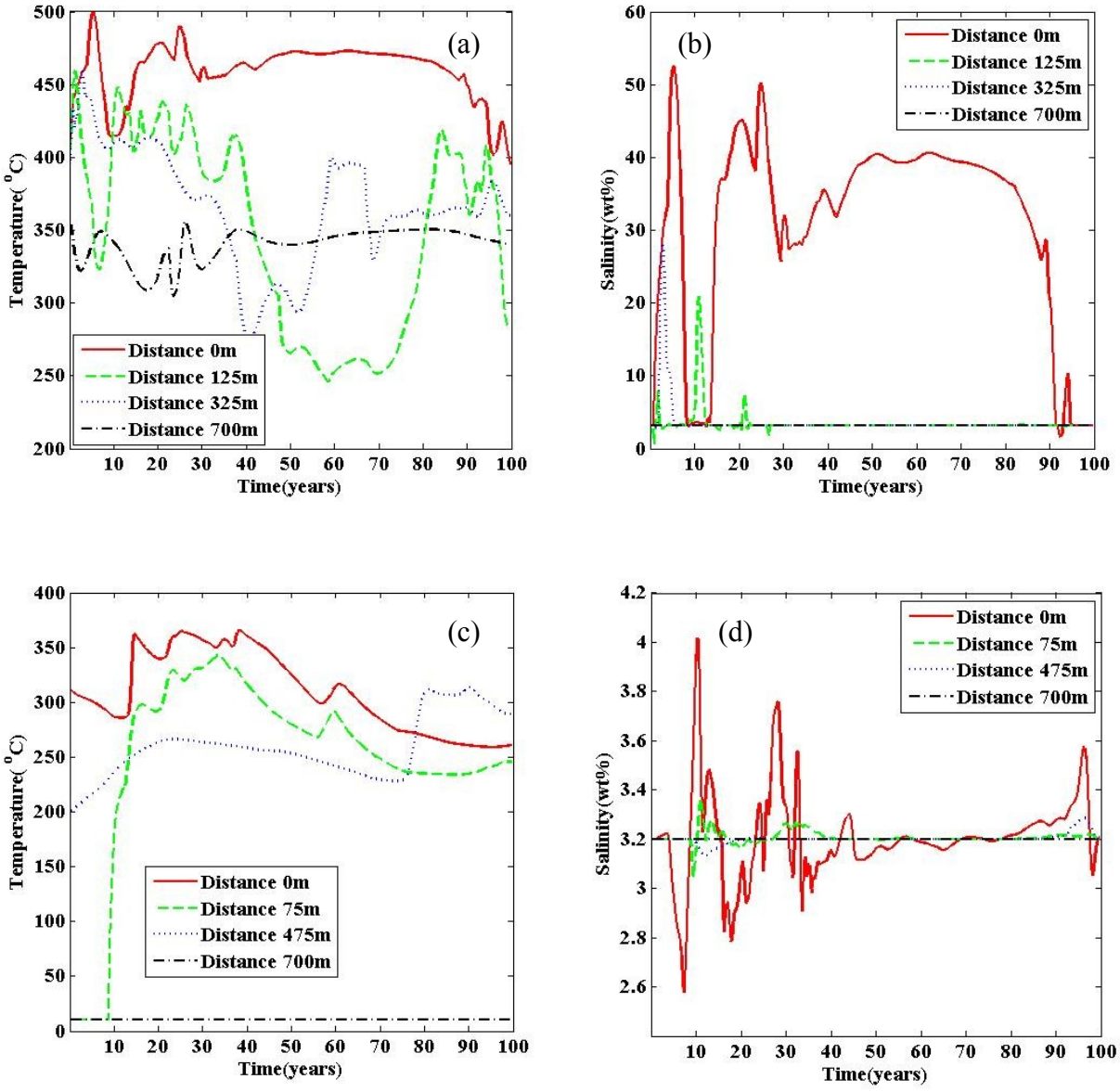

Figure 4.11 (a) Bottom temperature (b) bottom salinity (c) seafloor temperature (d) seafloor salinity for a heat input with replenishment.

CHAPTER 5: DISCUSSION

Temperature and salinity are perhaps the two most measurable essential parameters of hydrothermal circulation at mid ocean ridges that reflect and integrate the physical and chemical processes occurring there. Temperature as an indicator of changes of hydrothermal circulation reflects the cooling of the magma bodies, permeability changes, rock seafloor reactions, and biogeochemical reactions [*Scheirer et al.,* 2006]. Salinity reflects the occurrence of phase separation and hence provides insight into temperature and pressure conditions at depth. The resulting salinity of hydrothermal vents is affected by mixing processes, which may be affected by the permeability distribution in the crust. Volcanic eruptions, dike intrusion, earthquakes can also cause temperature and salinity variations by changing both temperature and permeability within the circulation system. Hence it is often difficult to infer how changes in temperature and salinity at the seafloor relate to changes in subsurface conditions.

In the preceding chapters of this thesis, I investigated the link between time dependent magmatic heat transfer and two-phase hydrothermal circulation at a mid-ocean ridge axis. In particular, I explored how bottom and seafloor temperature and salinity would respond to a variety of time-varying heat input functions. A constant heat flux simulation using 130 W/m^2 was used to compare the results from the time-varying basal condition with a constant heat flux condition. To compare the results of different basal heat inputs, I considered a two-dimensional open-top rectangular box 1.5 km deep and 4 km long with homogeneous permeability of 10^{-13} m^2 and with temperature and pressure at top boundary corresponding to seafloor conditions of 10°C, 25MPa, respectively. This geometry and set of boundary conditions approximate conditions at the East Pacific Rise 9°50′N hydrothermal site [e.g., *Lowell et al.,* 2012, 2013].

There are three principal findings from the simulations in chapter 4.

(1) Seafloor temperatures do not respond in a clear way to changes in bottom heat flux. Seafloor temperatures are influenced by mixing between upward flowing hot fluids and downward flowing cold fluids as well as by lateral diffusion, and these processes dampen the response of the seafloor temperature.

(2) Seafloor salinities do respond more clearly to changes in the thermal regime at depth. For periodic and other oscillatory heat inputs, the main reason for fluctuations between slightly above and slightly below 3.2wt% NaCl vent fluid is the exchange of the VDF and BDF as the heat flux changes over time. During phase separation a high salinity brine becomes a conjugate of a low salinity vapor. A low salinity vapor with lower density rises easily and mixes with seawater resulting in a low salinity response at the seafloor. On the other hand, the high salinity brine with higher density ascends as a result of the unsteady nature of the high Rayleigh number convection. During ascent the brine loses a certain amount of salinity by mixing with seawater, and the BDF reaches at the seafloor. As an example, seafloor salinities of the constant heat flux and replenishment case fluctuate between 2.6~4.2 wt% NaCl when the bottom salinities are above 30 wt% NaCl [Figure 4.2 and Figure 4.11]. In the case of oscillatory heat flux, the seafloor salinities exhibit not only the exchanges of VDF and BDF but also reflect the response of the characteristics of the heat flux input function.

(3) Seafloor salinities exhibit a time delay relative to changes at depth. The main reason for the delay is the ascent time of the fluid. It takes less than a decade for the fluid transport from the bottom of the system to the seafloor. In the case of decaying heat flux, the time delay of the last BDF was about 5 years [Figure 4.10]. As the heat flux decreases from the region of the two-

phase flow to the single-phase flow, which occurs for all the cases shown in section 4.4, the change in seafloor salinity occurs later than bottom salinity. The main affect of reducing the bottom heat flux to a value where phase separation is not sustained is to gradually flush the basal brine out of the system. In this case seafloor salinity rises to as much as 3.65 wt% NaCl [Figure 4.10], and the salinity gradually returns to the seawater value.

Many observational studies of temperature and salinity (often expressed in the literature as Cl content rather than wt% NaCl) at the East Pacific Rise near 9°50′ N and the Main Endeavour Field on the Juan de Fuca Ridge PR and Endeavour have shown strong evidence of rapid temperature and/or salinity changes with tim e [*Von Damm,* 2004; *Scheirer et al.,* 2006; *Sohn et al.,* 1998; *Butterfield,* 1994; *Lilley et al,* 2003; *Seyfried et al.,* 2005]. These are shown in Figure 5.1 and Figure 5.2.

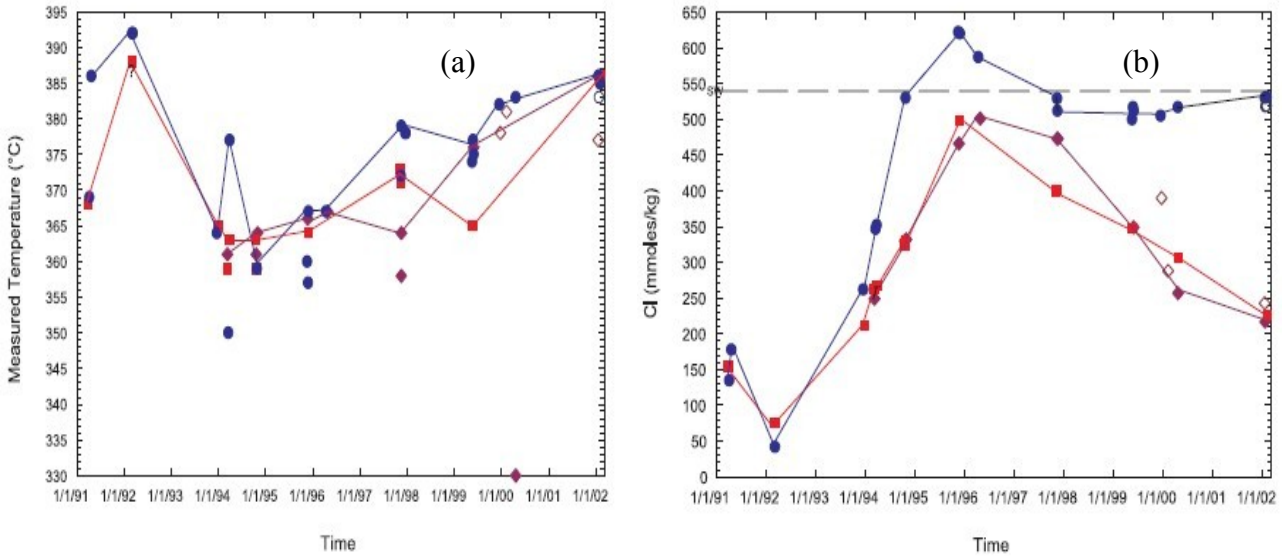

Figure 5.1 Vent fluid temperature (a) and salinity (b) data from the East Pacific Rise 9°50'N. Data from Von Damm, 2004; P (blue), Bio 9 (red), and Bio 9' (dark red) are the different vents. Bio 9 and P vent are separated by about 60 m. After the eruption in 1991-1992 temperature increases rapidly while salinity decreases; both show a gradual return to pre-event condition. (The figure reprinted with permission of the American Geophysical Union).

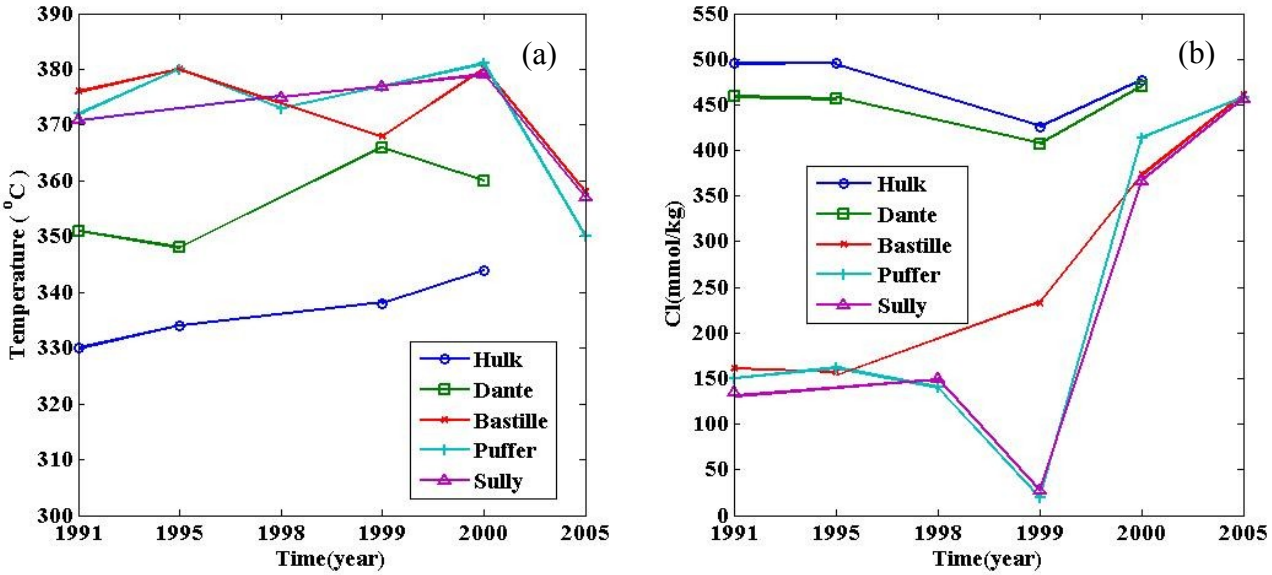

Figure 5.2 Vent fluid temperature (a) and salinity (b) data from the Main Endeavour Field. Data from *Lilley et al*. [2003] and *Foustoukos et al.* [2009]. After the eruption in 1999 temperature increases rapidly while salinity decreases. Hulk and Dante are in the northern part of the vent field whereas Puffer, Bastille and Sully are in the southern part of the vent field, which extends approximately 400 m in length.

A key question is whether these observed changes can be related to the temporal changes in vent temperature and salinity described by the models developed here.

This study focused on the evolution of temperature and salinity at the seafloor in response to changing heat flux at the base of the circulation system. The results indicate that seafloor temperature itself is not sufficient to resolve the reason of changes in basal heat flux. On the other hand, salinity is a relatively good indicator. Figure 4.3 shows that oscillatory heat flux input on time scales of several years would be manifested in seafloor salinity variations. If the system decays, a significant discharge of BDF occurs, after which the seafloor salinity would return to the seawater value [Figure 4.10]. Salinity can thus be an indicator of changes in the subsurface heat flux. The observations shown in Figure 5.1 and Figure 5.2 cannot be easily related to the perturbations and responses investigated in the models described in this thesis, however. These perturbations are typically related to discrete magmatic events that may or may not have resulted in a magmatic eruption. These events appear to affect the thermal and permeability structures at

relatively shallow depths in the system [e.g., *Germanovich et al.,* 2011], hence enabling a much more rapid response of both temperature and salinity than results from changes in heat flux at the base of the system.

CHAPTER 6: CONCLUSIONS AND RECOMMENDATIONS FOR FUTURE WORK

In this thesis, I studied the coupling of a two-phase NaCl-H_2O seafloor hydrothermal system with magmatic processes. The effects on the magma heat flux with two-phase hydrothermal processes were investigated. Different mathematical functions were used as magmatic heat input. Time dependent magmatic heat input was modeled as constant, oscillating, and decaying heat flux. The calculated heat outputs from *Liu and Lowell* [2009] were also used to estimate heat transfer from a convecting, crystallizing, replenished magma chamber to the hydrothermal system.

Constant heat flux represents an idealistic scenario that can be used to compare with results from cases with time-varying heat input. In this case, the temperature and salinity near the bottom of the hydrothermal system show large fluctuations at the center of AMC that decrease towards the end of the AMC. The surface temperature of the ascending plumes is somewhat lower than that at the bottom because of mixing and the magnitude of the oscillation is somewhat damped. Both VDF and BDF fluids discharge at the surface at various times in response of the changes of the bottom salinity. These oscillations are a natural consequence of the large Rayleigh number in the system and hence such oscillations cannot be used to suggest temporal variations in the basal heat flux.

At the bottom of the hydrothermal system, temperature and salinity of the fluids show clear variations with the changing heat flux at the base. The seafloor temperatures, however, though varying with time, show no correlation with temporal variations in the basal heat flux.

Analytically calculated heat outputs from the magma chamber based on the results of *Liu and Lowell* [2009] are applied to the system. The two-phase flow decays rapidly in the case of magma heat output without replenishment. Bottom temperature and salinity follows the decaying

heat flux. The seafloor salinity is clearly out of phase with the fluctuations of the bottom salinity. The two-phase flow rebounds when the replenishment of the magma chamber occurs and heat flux is maintained at a high value. The heat transport of the hydrothermal system is extended as a result of replenishment. Except for an initial period during which the heat flux decays, this situation is similar to the constant heat flux case.

In summary, following results are obtained from the simulation results:

1. The changes in bottom temperature and salinity closely follow the temporal variations in magmatic heat inputs.
2. The surface temperature response is severely damped and high frequency variations in heat flow are not detected.
3. Above regions where phase separation occurs, surface salinity variations may be recorded in response to changing conditions at depth, but these are smaller in amplitude than the changes at depth.
4. The response of surface temperature and salinity to changes in basal heat flux is significantly delayed.

As recommendation for future work, there are few things to be considered. First, the improvement in FISHES is needed to consider temperatures greater than 500°C. The FISHES could not read the temperature greater than 500°C and stopped at the base temperature of 550°C for several simulations. This problem can be solved from a new version by the author in the future. Second, numerical simulations at higher resolution are needed in the future. All of these results of the simulations were run by 25m by 25m. The heat flux needed for the two-phase flow was 100 W/m^2 according to the simulation result. The result, however, can be different for the higher resolution of the simulation. For example, phase separation did not occur at the resolution

of 50m by 50m for the heat flux 100~150 W/m^2(not included in thesis). The higher resolution such as 10m by 10m expects to lower heat flux needed for the phase separation. Finally, the effects of varying permeability are not included. In this thesis, homogeneous $10^{-13}m^2$ permeability was used. Various heterogeneous permeabilities may affect the result of the simulation. Such variations could include the incorporation of layer 2A extrusives and highly permeable faults or fractures. Time dependent permeability could result from tectonic and magmatic events as well as from mineral precipitation and dissolution.

REFFERENCES

Anderko, A., and K. Pitzer (1993), Equation-of-state representation of phase equilibria and volumetric properties of the system NaCl-H2O above 573K, *Geochim. Cosmochim. Acta*, 57, 1657-1680.

Anderson, R. N. and M.D. Zoback (1982), Permeability, underpressures, and convection in the oceanic crust near the Costa Rica Rift, eastern equatorial pacific. *J. Geophys. Res.,* 87:2860-2868.

Anderson, R. N., M.D. Zoback, S.H. Hickman and R.L. Newmark (1985a), Permeability versus depth in the upper oceanic crust: in situ measurements in DSDP Hole 504B, eastern equatorial Pacific. *J. Geophys. Res.,* 90:3659-3669.

Anderson, R. N., M.D. Zoback, S.H. Hickman and R.L. Newmark (1985b), Permeability versus depth in the upper oceanic crust: *in situ* measurements in Deep Sea Drilling Project Hole 504B, eastern equatorial Pacific. *In* Anderson, R. N., Honnorez, J., Becker, K., et al., *Init. Repts. DSDP,* 83: Washington (U.S. Govt. Printing Office), 429-442.

Archer, D. (1992), Thermodynamic properties of the NaCl+H2O system II. Thermodynamic properties of NaCl (aq), NaCl·2H2O (cr), and phase equilibria, *J. Phys. Chem. Ref. Data, 21,* 793-820.

Batiza, R. and Niu, Y. (1992), Petrology and Magma Chamber Processes at the East Pacific Rise ~9^{o}30'N. *Journal of Geophysical Research 97(B5):* doi: 10.1029/92JB00172.

Bai, W., W. Xu, and R. P. Lowell (2003), The dynamics of submarine geothermal heat pipes, *Geophys. Res. Lett., 30*(3), 1108, doi:10.1029/2002GL016176.

Baker, E.T. 2007. Hydrothermal cooling of mid-ocean ridge axes: Do measured and modeled heat fluxes agree? *Earth and Planetary Science Letters* 263:140–150, http://dx.doi.org/10.1016/j.epsl.2007.09.010.

Bear, J., (1972), Dynamics of fluids in porous media*, Elsevier*, N.Y.

Becker, K. and H. Sakai (1989). Measurements of the permeability of the sheeted dikes in hole 504B, ODP LEG 111. *Proceedings of the Oceanic Drilling Program, Scientific Results,* Vol.111.

Berg, R. R. (1970), Method for determining permeability from reservoir rock properties: *Transactions of the American Institute of Mechanical Engineers, 146, 54–67.*

Berndt, M. E., and W. E. Seyfried, Jr. (1990), Boron, bromine, and other trace elements as clues to the fate of chlorine in mid-ocean ridge vent fluids*, Geochim. Cosmochim. Acta, 54,* 2235-2245.

Bejan, A. (1995), Convection heat transfer, *Wiley & Sons, Inc*.

Bischoff, J., and R. Rosenbauer (1984), The critical point and two-phase boundary of seawater, 200° - 500 °C, *Earth Planet. Sci. Lett., 68*, 172-180.

Bischoff, J., and R. Rosenbauer (1988), Liquid-vapor relations in the critical region of the system NaCl-Hz0 from 380 to 415°C: A refined determination of the critical point and two-phase boundary of seawater, *Geochimica et Cosmochimica Acla* Vol. 52. pp. 212l-2126.

Bischoff, J. L., and K. S. Pitzer (1989), Liquid-vapor relations for the system NaCl-H2O: Summary of the P-T-x surface from 300° to 500°C, *Am. J. Sci., 289*, 217-248.

Bodvarsson, G., and R. P. Lowell (1972), Ocean-floor heat flow and the circulation of interstitial waters, *J. Geophys. Res., 77*, 4472-4475.

Bower, K. M., and G. Zyvoloski (1997), A numerical model for thermo-hydro-mechanical coupling in fractured rock, *Int. J. Rock Mech. Min. Sci., 34*, 1201-1211.

Bredehoeft, J.D., and Norton, D.L. (1990), The role of fluids in crustal processes: National Research Council Study in Geophysics, *National Academy Press,* Washington, D.C., 170 p.

Brikowski, T., and D. Norton (1989), Influence of magma chamber geometry on hydrothermal activity at mid-ocean ridges, *Earth Planet. Sci. Lett., 93*, 241-255.

Buck, W. R., P. T. Delaney, J. A. Karson, and Y. Lagabrielle, editors, (1998), *Faulting and magmatism at mid-ocean ridges, Geophys. Monogr. Ser., v. 106,* 348 pp., American Geophys. Union, Washington, D. C.

Butterfield, D. A., R. E. McDuff, M. J. Mottl, M. D. Lilley, J. E. Lupton, and G. J. Massoth (1994), Gradients in the composition of hydrothermal fluids from the Endeavour segment vent field: Phase separation and brine loss, *J. Geophys. Res., 99,* 9561-9583.

Butterfield D.A., I. R. Jonasson, G. J. Massoth, R. A. Feely, K. K. Roe1, R. E. Embley, J. F. Holden, R. E. McDuff, M. D. Lilley and J. R. Delaney (1997), Seafloor eruptions and evolution of hydrothermal fluid chemistry, *Phil. Trans. R. Soc.* A, 355, 369-386.

Canales, J.P., S.C. Singh, R.S. Detrick, S.M. Carbotte, A. Harding, G.M. Kent, J.B. Diebold, J. Babcock, and M.R. Nedimovic (2006), Seismic evidence for variations in axial magma chamber properties along the southern Juan de Fuca Ridge, *Earth. Planet. Sci. Lett.*, *246*, 353-366.

Cann, J., and M. Strens (1982), Black smokers fuelled by freezing magma, *Nature*, 298, 147–149, doi:10.1038/298147a0.

Carlson,R.L. (2011), The effect of hydrothermal alteration on the seismic structure of the upper oceanic crust: Evidence from Holes 504B and 1256D. *AGU,Vol*. 12, NO. 9,doi:10.1029.

Cathles, L. M. (1977), An analysis of the cooling of intrusive by ground-water convection which

includes boiling, *Econ. Geol., 72*, 804-826.

Collier, J.S. and M.C. Sinha (1990), Seismic images of a magma chamber beneath the Lau Basin back-arc spreading centre, *Nature*, *346*, 646-648.

Corey, A. T. (1954), The Interrelation Between Gas and Oil Relative Permeabilities, *Prod. Monthly* 19 (1): 38–41.

Coumou, D., T. Driesner, S. Geiger, C. A. Heinrich, and S. Matthäi (2006), The dynamics of mid-ocean ridge hydrothermal systems: Splitting plumes and fluctuating vent temperatures, *Earth Planet. Sci. Lett., 245*, 218-235.

Coumou, D. (2008), Numerical simulation of fluid flow in mid-ocean ridge hydrothermal systems, Ph.D. thesis, ETH Zurich, Zurich, Switzerland.

Coumou, D., T. Driesner, and C. Heinrich (2008a), Heat transport at boiling, near-critical conditions, *Geofluids, 8*, 208-215.

Coumou, D., T. Driesner, and C. Heinrich (2008b), The structure and dynamics of mid-ocean ridge hydrothermal systems, *Science, 321*, 1825-1828.

Coumou, D., T. Driesner, P. Weis, and C. Heinrich (2009), Phase separation, brine formation, and salinity variation at Black Smoker hydrothermal systems, *J. Geophys. Res., 114*, B03212, doi:10.1029/2008JB005764.

Dake, L.P. (1977), Fundamentals of Reservoir Engineering, *Elsevier Scientific Publishing Company, Amsterdam.*

Detrick, R. S., P. Buhl, E. Vera, J. Mutter, J. Orcutt, J. Madsen, and T. Brocher (1987), Multichannel seismic imaging of a crustal magma chamber along the East Pacific Rise, *Nature, 326*, 35-41.

Driesner T. and Geiger S. (2007), Numerical simulation of multiphase fluid flow in hydrothermal systems. *Reviews in Mineralogy & Geochemistry*, Vol. 65, pp. 187-212.

Driesner, T., and C. Heinrich (2007), The system H2O-NaCl. Part I: Correlation formulae for phase relations in temperature-pressure-compositions pace from 0 to 1000 °C, 0 to 5000 bar, and 0 to 1 XNaCl, *Geochim. Cosmochim. Acta, 71*, 4880-4901.

Elder, J. W. (1965), Physical processes in geothermal areas, in *Terrestrial Heat Flow, Geophys. Monogr. Ser.,* vol. 8, edited by W. H. K. Lee, pp. 211-239, AGU, Washington, D. C.

Elder, J. (1967), Transient convection in a porous medium, *J. Fluid Mech., 27*, 609-623.

Faust, C. R., and J. W. Mercer (1979), Geothermal reservoir simulation: 1. Mathematical models for liquid- and vapor-dominated hydrothermal systems, *Water Resour. Res., 15*, 23-30.

Fehn, U., and L. Cathles (1979), Hydrothermal convection at slow-spreading midocean ridges, *Tectonophysics, 55,* 239-260.

Fehn, U., and L. Cathles (1986), The influence of plate movement on the evolution of hydrothermal convection cells in the oceanic crust, *Tectonophysics, 125*, 289-312.

Fehn, U., K. E. Green, R. P. Von Herzen, and L. M. Cathles (1983), Numerical models for the hydrothermal field at the Galapagos Spreading Center, *J. Geophys. Res., 88*, 1033-1048.

Fisher. A.T. (1998), Permeability within basaltic oceanic crust, *Rev Geophys.,* 36, 143-182.

Foustoukos, D. I., N. J. Pester, K. Ding, and W. E. Seyfried Jr (2009), Dissolved carbon species in associated diffuse and focused flow hydrothermal vents at the Main Endeavour Field, Juan de Fuca Ridge: Phase equilibria and kinetic constraints, *Geochem. Geophys. Geosyst., 10*, Q10003, doi:10.1029/2009GC002472.

Foutaine, F. J., and W. S. D. Wilcock (2009), Two-dimensional numerical models of open-top hydrothermal convection at high Rayleigh and Nusselt numbers: Implications for mid-ocean ridge hydrothermal circulation, *Geochem. Geophys. Geosyst., 8*, Q07010,doi:10.1029/2007GC001601.

Fontaine, F., W. Wilcock, and D. Butterfield (2007), Physical controls on the salinity of midocean ridge hydrothermal vent fluids, *Earth Planet. Sci. Lett., 257*, 132-145.

Fornari, D. J., K. L. Von Damm, T. K. P. Gregg, M. Lilley, G. Levai, A. Bray, R. M. Haymon, M. R. Perfit, and R. Lutz (1998b), Time-series temperature measurements at high-temperature hydrothermal vents, East Pacific Rise 9°49'-51'N: Evidence for monitoring a crustal cracking event, *Earth Planet. Sci. Lett., 160,* 419-431.

Geiger, S., T. Driesner, C. A. Heinrich, and S. K. Matthäi (2006a), Multiphase thermohaline convection in the Earth's crust: I. A new finite element-finite volume solution technique combined with a new equation of state for NaCl-H2O, *Transp. Porous Media, 63*, 399-434.

Geiger, S., T. Driesner, C. A. Heinrich, and S. K. Matthäi (2006b), Multiphase thermohaline convection in the Earth's crust: II. Benchmarking and application of a finite element-finite volume solution technique with a NaCl-H2O equation of state, *Transp. Porous Media, 63*, 435-461.

Gente, P., J.M. Auzende, V. Renard, Y. Fouquet, and D. Bideau (1986), Detailed geological mapping by submersible of the East Pacific Rise axial graben near 13°N, *Earth Planet. Sci. Lett.*, *78*, 224-236.

German, C. R., J. Lin, and L. M. Parson, editors, (2004), Mid-ocean ridges: Hydrothermal interactions between the lithosphere and oceans, *Geophys. Monogr. Ser., v. 148,* 318 pp., American Geophys. Union, Washington, D. C.

Germanovich, L., R. Lowell, and D. Astakhov (2000), Stress-dependent permeability and the formation of seafloor event plumes, J. Geophys. Res., 105, 8341–8354, doi:10.1029/1999JB900431.

Germanovich, L. N., Lowell, R. P., and Astakhov, D. K. (2001), Temperature-dependent permeability and bifurcations in hydrothermal flow, Journal of Geophysical Research, Vol. 106, No. B1, pp. 473 – 495.

Germanovich, L.N., Lowell,R.P. and Ramondenc, P. (2009), Magmatic origin of the March 1995 earthquake swarm at 9°50′ N, East Pacific Rise. J. Geophys. Res.

Germanovich, L.N., R.P. Lowell, and P. Ramondenc. (2011), Magmatic origin of hydrothermal response to earthquake swarms: Constraints from heat flow and geochemical data at 9°50'N, East Pacific Rise. *Journal of Geophysical Research* 116, B05103, http:// dx.doi.org/10.1029/2009JB006588.

Ghiorso, M.S. and Sack ,R.O. (1995), Chemical mass transfer in magmatic processes. IV. A revised and internally consistent thermodynamic model for the interpolation and extrapolation of liquid-solid equilibria in magmatic systems at elevated temperatures and pressures, Contrib. Mineral. Petrol., 119, 197-212.

Han, Liang (2011), Exploring two-phase hydrothermal circulation at a seafloor pressure of 25MPa: Application for EPR 9°50’ N. *Master thesis. Virginia Tech.*

Hannington, M. D., I. R. Jonasson, P. M. Herzig, and S. Petersen (1995), Physical and chemical processes of seaflorr mineralization at mid-ocean ridges, in *Seafloor Hydrothermal Systems: Physical, Chemical, Biological, and Geological Interactions, Geophys. Monogr. Ser.,* vol. 91, edited by S. E. Humphris, R. A. Zierenberg, L. S. Mullineaux, and R. E. Thomson, pp. 115-157, AGU, Washington, D. C.

Haymon R.M. (1983), Growth history of black smoker hydrothermal chimneys, *Nature*, 301, 695-98.

Haymon, R. M., D. J. Fornari, M. H. Edwards, S. Carbotte, D. Wright, and K. C. Macdonald (1991), Hydrothermal vent distribution along the East Pacific Rise crest (9°09’-54’N) and its relationship to magmatic and tectonic processes on fast-spreading mid-ocean ridges, *Earth Planet. Sci. Lett., 104*, 513-534.

Haymon, R. M., D. J. Fornari, K. L. Von Damm, M. D. Lilley, M. R. Perfit, J. M. Edmond, W. C. Shanks, III, R. A. Lutz, J. M. Grebmeier, S. Carbotte, D. Wright, E. McLaughlin, M. Smith, N. Beedle, and E. Olson (1993), Volcanic eruption of the mid-ocean ridge along the East Pacific Rise crest at 9°45’-52’N: Direct submersible observations of seafloor phenomena associated with an eruption even in April, 1991, *Earth Planet. Sci. Lett., 119*, 85-101.

Horton, E. W., and F. T. Rogers, Jr. (1945), Convection currents in porous media, *J. Appl. Phys.,*

16, 367-370.

Humphris, S. E., R. A. Zierenberg, L. S. Mullineaux, and R. E. Thomson, editors, (1995), *Seafloor hydrothermal systems: Physical, chemical, biological, and geological interactions, Geophys. Monogr. Ser., v. 91,* 466 pp., American Geophys. Union, Washington, D. C.

Huppert, H.E. and R.S.J. Sparks (1988), The generation of granitic magmas by intrusion of basalt into continental crust, *J. petrology*, *29*, 599-624.

Ingebritsen, S. E., and D. O. Hayba (1994), Fluid flow and heat transport near the critical point of H2O, *Geophys. Res. Lett., 21*, 2199-2203.

Jarvis, G.T. and W.R. Peltier (1989), Convection models and geophysical observations, in *Mantle Convection*: *Plate Tectonics and Global Dynamics*, ed. W.R. Peltier, Gordon and Breach Science Publishers, 479-595.

Jupp, T., and A. Schultz (2000), A thermodynamic explanation for black smoker temperatures, *Nature, 403*, 880-883.

Kawada, Y., S. Yoshida, and S. I. Watanabe (2004), Numerical simulations of mid-ocean ridge hydrothermal circulation including the phase separation of seawater, *Earth Planets Space, 56*, 193-215.

Kelly, D. S., and J. R. Delaney (1987), Two-phase separation and fracturing in mid-ocean ridge gabbros at temperatures greater than 700 °C, *Earth Planet. Sci. Lett., 83*, 53-66.

Kelly, DS. (1996), Methane-rich fluids in the oceanic crust. *J. Geophysics Res.* 101:2943-62.

Kelley, DS., Baross, J.A., Delaney, J.R. (2002), Volcanoes, Fluids, and Life at Mid-Ocean Ridge Spreading Centers. *Annu. Rev. Earth Planet Science,* 30, 385-491.

Kent, G.M., A.J. Harding, and J.A. Orcutt (1990), Evidence for a smaller magma chamber beneath the East Pacific Rise at 9º30´N, *Nature*, *344*, 650-652.

Kissling, W. (2005a), Transport of three-phase hyper-saline brines in porous media: theory and code implementation, *Transp. Porous Media, 61*, 25-44.

Kissling, W. (2005b), Transport of three-phase hyper-saline brines in porous media: examples, *Transp. Porous Media, 60*, 141-157.

Lapwood, E., Convection of a fluid in a porous media, *Proc. Cambridge philos. Soc., 44*, 508-521.

Larson, B. I., E. J. Olson, and M. D. Lilley (2007), In situ measurement of dissolved chloride in high temperature hydrothermal fluids, *Geochim. Cosmochim. Acta, 71*, 2510-2523.

Lewis, K. C., and R. P. Lowell (2004), Mathematical modeling of phase separation of seawater near an igneous dike, *Geofluids, 4*, 197-209.

Lewis, K. C. (2007), Numerical modeling of two-phase flow in the sodium chloride-water system with applications to seafloor hydrothermal systems, Ph.D. thesis, Ga. Inst. of Technol., Atlanta.

Lewis, K. C., and R. P. Lowell (2009a), Numerical modeling of two-phase flow in the NaCl-H_2O system: Introduction of a numerical method and benchmarking, *J. Geophys. Res., 114*, B05202, doi:10.1029/2008JB006029.

Lewis, K. C., and R. P. Lowell (2009b), Numerical modeling of two-phase flow in the NaCl-H_2O system: 2. Examples, *J. Geophys. Res., 114*, B08204, doi:10.1029/2008JB006030.

Liu, L., and R. P. Lowell (2009), Models of hydrothermal heat output from a convecting, crystallizing, replenished magma chamber beneath an oceanic spreading center, *J. Geophys. Res., 114,* B02102, doi:10.1029/2008JB005846.

Liu, L. (2010), Heat Transfer from a Convecting Crystallizing, Replenished Magmatic Sill and Its Link to Seafloor Hydrothermal Heat Output, Ph.D. Thesis, 291 p., *Georgia Institute of Technology*, Atlanta.

Lilley, M. D., D. A. Butterfield, J. E. Lupton, and E. J. Olson (2003), Magmatic events produce rapid changes in hydrothermal vent chemistry, *Nature, 422,* 878-881.

Lister, C. R. B. (1972), On the thermal balance of a mid-ocean ridge, *Geophys. J. R. Astron. Soc., 26*, 515-535.

Lister, C. R. B. (1974), On the penetration of water into hot rock, *Geophys. J. R. Astron. Soc., 39,* 465-509.

Lowell, R. P. (1975), Circulation in fractures, hot springs, and convective heat transport on mid ocean ridge crests, *Geophys. J. R. Astron. Soc., 40*, 351-365.

Lowell, R., and P. Rona (1985), Hydrothermal models for the generation of massive sulfide ore deposits, *J. Geophys. Res.,* 90, 8769 – 8783, doi:10.1029/JB090iB10p08769.

Lowell, R. P., and D. K. Burnell (1991), Mathematical modeling of conductive heat transfer from a freezing convecting magma chamber to a single-pass hydrothermal system: Implications for sea floor black smokers, *Earth Planet. Sci. Lett.*, *104*, 59-69.

Lowell, R. P., and L. N. Germanovich (1994), On the temporal evolution of high-temperature hydrothermal systems at ocean ridge crests, *J. Geophys. Res., 99*, 565-575.

Lowell, R. P. and W. Xu (2000), Sub-critical two-phase seawater convection near a dike, *Earth Planet. Sci. Lett., 174*, 385-396.

Lowell, R.P. and Rona, P.A. (2004), Hydrothermal Activity. *Encyclopedia of Geology*, *Elervier*,V.5,362-372.

Lowell, R. P., and L. N. Germanovich (2004), Hydrothermal processes at mid-ocean ridges: Results from scale analysis and single-pass models, in *Mid-Ocean Ridges: Hydrothermal Interactions Between the Lithosphere and Oceans, Geophys. Monogr.Ser.,* vol. 148, edited by C. German, J. Lin, and L. M. Parson, pp. 219-244, AGU, Washington, D. C.

Lowell, R.P. S.R. Gosnell and Y. Yang (2007), Numerical simulations of single-pass hydrothermal convection at mid-ocean ridges: Effects of the extrusive layer and temperature dependent permeability, *Geochem. Geophys. Geosystems*, 8, Q10011, doi:10.1029/2007GC001653.

Lowell, R.P., B.W. Crowell, K.C. Lewis, and L. Liu (2008), Modeling multiphase, multi-component processes at oceanic spreading centers, in Magma to Microbe: Modeling Hydrothermal Processes at Oceanic Spreading Centers, *Geophys. Monogr. Ser.,* v. 178, ed. by R.P. Lowell, J.S. Seewald, A. Metaxas, and M.R. Perfit, p. 15-44, American *Geophys. Union*, Washington, DC.

Lowell, R.P., A. Farough, L.N. Germanovich, L.B. Hebert, and R. Horne (2012, 2013), A vent-field-scale model of the East Pacific Rise 9°50'N magma-hydrothermal system. *Oceanography* 25(1):158–167, http://dx.doi.org/10.5670/oceanog.

Macdonald, K.C., K. Becker, F.N. Spiess, and R.D. Ballard (1980), Hydrothermal heat flux of the "black smokers" vents on the East Pacific Rise, *Earth Planet. Sci. Lett*., 48, 1-7.

MacInnis, S. L. Han, R.P. Lowell, J.D. Rimsstidt, R.J. Bodnar (2012a), The role of fluid phase immiscibility in quartz dissolution and precipitation in sub-seafloor hydrothermal systems, *Earth Planet. Sci. Lett.* 321-322:139-151. doi:10.1016/j.epsl.2011.12.037.

MacInnis, S. L. Han, R.P. Lowell, J.D. Rimsstidt, R.J. Bodnar (2012b), Quartz precipitation and fluid inclusion characteristics in sub-seafloor hydrothermal systems associated with volcanogenic massive sulfide deposits, *Centr. Euro. J. Geosc. Vol.4,* pp 275-286., doi: 10.2478/s13533-011-0053-z.

MacLeod CJ, Yaouancq G. (2000), A fossil melt lens in the Oman ophiolite: implications for magma chamber processes at fast-spreading ridges. *Earth Planet. Sci. Lett.* 176:357–73.

Matthäi, S. K., et al. (2007), Numerical simulations of multiphase fluid flow in structurally complex reservoirs, in Structurally Complex Reservoir, edited by S. J. Jolley et al., *Geol. Soc. Spec. Publ., 292*, 405-429.

Mckenzie, D. P. (1965), Some remarks on heat flow and gravity anomalies, in *Terrestrial Heat Flow, Geophys. Monogr. Ser.,* vol. 8, edited by W. H. K. Lee, pp. 240-260, AGU, Washington,

D. C.

Nelson, P.H. (1994), Permeability-porosity relationships in sedimentary rocks, *Log Analyst,* 35: 38 – 62.

Nehlig, P. (1991), Salinity of oceanic hydrothermal fluids: a fluid inclusion study, *Earth Planet. Sci. Lett., 102*, 310-325.

Nield, D. A. (1968), Onset of thermohaline convection in a porous medium, *Water Resour. Res., 1*, 553-560.

Palliser, C., and R. Mckibbin (1998a), A model for deep geothermal brines, I: T-p-X state-space description, *Transp. Porous Media, 33*, 65-80.

Palliser, C., and R. Mckibbin (1998b), A model for deep geothermal brines, II: Thermodynamic properties—Density, *Transp. Porous Media, 33*, 129-154.

Palliser, C., and R. Mckibbin (1998c), A model for deep geothermal brines, III: Thermaodynamic properties—Enthalpy and viscosity, *Transp. Porous Media, 33*, 155-171.

Parker, R. L., and D. W. Oldenburg (1973), Thermal model of ocean ridges, *Nature, Phys. Sci., 242*, 137-139.

Patankar, S. (1980*), Numerical Heat Transfer and Heat Flow,* Taylor and Francis, London.

Perfit, M.R., D.J. Fornari, M.C. Smith, J.F. Bender, C.H. Langmuir, and N.W. Hayman. (1994), Small-scale spatial and temporal variations in mid-ocean ridge crest magmatic processes. *Geology* 22:375–379.

Ramondenc, P., L. N. Germanovich, K. L. Von Damm, and R. P. Lowell (2006), The first measurements of hydrothermal heat output at 9°50'N, East Pacific Rise*, Earth Planet. Sci. Lett., 245*, 487-497.

Rona., P. A., C. W. Devey, J. Dyment, and B. J. Murton, editors, (2010), Diversity of hydrothermal systems on slow spreading ocean ridges, *Geophys. Monogr. Ser., v. 188,* 440 pp., American Geophys. Union, Washington, D. C.

Sabersky, R.H. and Acosta, A.J. (1971), Fluid Flow. *Macmillan Publishing Co. Inc*.

Scheirer, D. S., T. M. Shank, and D. J. Fornari (2006), Temperature variations at diffuse and focused flow hydrothermal vent sites along the northern East Pacific Rise, *Geochem. Geophys. Geosyst.,7*, Q03002, doi:10.1029/2005GC001094.

Sclater, J. G., and J. Francheteau (1970), The implications of terrestrial heat-flow observations on current tectonic and geochemical models of the crust and upper mantle of the Earth, *Geophys. J. R. Astron. Soc., 20*, 509-542.

Sclater, J. G., C. Jaupart, and D. Galson (1980), The heat flow through the oceanic and continental crust and the heat loss of the Earth, *Rev. Geophys., 18*, 269-311.

Seyfried, W. E., Jr., M. E. Berndt, and D. R. Janecky (1986), Chloride depletions and enrichments in seafloor hydrothermal fluids: Constraints from experimental basalt alteration studies, *Geochim. Cosmochim. Acta, 50*, 469-475.

Seyfried, W. E., Jr., K. Ding, and M. E. Berndt (1991), Phase equilibria constraints on the chemistry of hot spring fluids at mid-ocean ridges, *Geochim. Cosmochim. Acta, 55*, 3559-3580.

Shank, T. M., D. J. Fornari, K. L. Von Damm, M. D. Lilley, R. M. Haymon, and R. A. Lutz (1998), Temporal and spatial patterns of biological community development at nascent deep-sea hydrothermal vents (9°50'N, East Pacific Rise), *Deep-Sea Research II, 45*, 465-515.

Singh, S.C., J.S. Collier, A.J. Harding, G.M. Kent, and J.A. Orcutt (1999), Seismic evidence for a hydrothermal layer above the solid roof of the axial magma chamber at the southern East Pacific Rise, *Geology*, *27*, 219-222.

Singh, S. C., W. C. Crawford, H. Carton, T. Seher, V. Combier, M. Cannat, J. P. Canales, D. Düsünür, J. Escartin, and J. M. Miranda (2006), Discovery of a magma chamber and faults beneath a Mid-Atlantic Ridge hydrothermal field, *Nature, 332*, 1029-1032.

Sinton, JM and Detrick, RS. (1992), Mid-ocean ridge magma chambers. *J. Geophys. Res.* 97:197–216.

Sohn, R. A., D. J. Fornari, K. L. Von Damm, J. A. Hildebrand, and S. C. Webb (1998), Seismic and hydrothermal evidence for a cracking even on the East Pacific Rise crest at 9°50'N, *Nature, 396*,159-161.

Spiess, F. N., K. C. Macdonald, T. Atwater, R. Ballard, A. Carranza, D. Cordoba, C. Cox, V. M. Diaz Garcia, J. Francheteau, J. Guerrero, J. Hawkins, R. Haymon, R. Hessler, T. Juteau, M. Kastner, R. Larson, B. Luyendyk, J. D. Macdougall, S. Miller, W. Normark, J. Orcutt, and C. Rangin (1980), East Pacific Rise: Hot springs and geophysical experiments, *Science, 207*, 1421-1433.

Steele-MacInnis, M., L. Han, R. P. Lowell, J. D. Rimstidt, and R. J. Bodnar (2011), The role of fluid phase immiscibility in quartz dissolution and precipitation in sub-seafloor hydrothermal systems, *Earth Planet. Sci. Lett.,* in review.

Strens, M. R., and J. R. Cann (1982), A model of hydrothermal circulation in fault zones at mid ocean ridge crests, *Geophys. J. R. Astron. Soc., 71*, 225-240.

Swift, S., M. Reichow, A. Tikku, M. Tominaga, and L. Gilbert, (2008), Velocity structure of upper ocean crust at Ocean Drilling Program Site 1256, *G3*, (doi:10.1029/2008GC002188).

Tanger, J., and K. Pitzer (1989), Thermodynamics of NaCl-H2O: A new equation of state for the near-critical region and comparisons with other equations for adjoining regions, *Geochim. Cosmochim. Acta, 53*, 973-987.

Tivey, M.K. (2007), Generation of seafloor hydrothermal vent fluids and associated mineral deposits. *Oceanography*, Vol. 20, No.1.

Tolstoy, M., F. Waldhauser, D. R. Bohnenstiehl, R. T. Weekly and W. -Y. Kim (2008), Seismic identification of along-axis hydrothermal flow on the East Pacific Rise, *Nature, 451*, 181-184.

Turcotte, D. L., and G. Schubert (1982), Geodynamics: Application of Continuum Physics to Geological Problems, *John Wiley,* Hoboken, N. J.

Turner, J.S. (1973), Buoyancy effects in fluids, *Cambridge University Press, London*.

Van Ark, E. M., R. S. Detrick, J. P. Canales, S. M. Carbotte, A. J. Harding, G. M. Kent, M. R. Nedimovic, W. S. D. Wilcock, J. B. Diebold, and J. M. Babcock (2007), Seismic structure of the Endeavour Segment, Juan de Fuca Ridge: Correlations with seismicity and hydrothermal activity, *J. Geophys. Res.*, *112*, B02401, doi: 10.1029/2005JB004210.

Van Baaren, J.P. (1979), Quick-look permeability estimates using sidewall samples and porosity logs, 6th annual European logging symposium transactions: *Society of Professional Well Log Analysts*, 19p.

Von Damm, K.L, Edmond,J.M., Grant,B.,Measures,C.I., Walden,B. and Weiss,R.F.(1985),Chemistry of submarine hydrothermal solutions at 21°N, East Pacific Rise. *Geochimica et Cosmochimica Acta* Vol.49,2197-2220.

Von Damm, K.L. (1995), Controls on the chemistry and temporal variability of seafloor hydrothermal fluids, in Seafloor Hydrothermal Systems, Geophys. Monogr. 91, ed. by S.E. Humphris, R.A. Zierenberg, L.S. Mullineaux, and R.E. Thomson, p. 222-247, Amer. Geophys. Union, Washington, DC.

Von Damm, K. L., L. G. Buttermore, S. E. Oosting, A. M. Bray, D. J. Fornari, M. D. Lilley, and W. C. Shanks, III (1997), Direct observation of the evolution of a seafloor 'black smoker' from vapor to brine, *Earth Planet. Sci. Lett., 149*, 101-111.

Von Damm, K. L. (2000), Chemistry of hydrothermal vent fluids from 9°-10°N, East Pacific Rise: "Time zero", the intermediate posteruptive period, *J. Geophys. Res., 105*, 11203-11222.

Von Damm, K. L., C. M. Parker, R. M. Gallant, and J. P. Loveless (2002), Chemical evolution of hydrothermal fluids from EPR 21° N: 23 year later in a phase separating world, *Eos Trans. AGU, 83*(47), Fall Meet. Suppl., Abstract V61B-1365.

Von Damm, K. L., and M. D. Lilley (2004), Diffuse flow hydrothermal fluids from 9°50'N East Pacific Rise: Origin, evolution and biogeochemical controls, in *The Subseafloor Biosphere at*

Mid-Ocean Ridges, Geophys. Monogr. Ser., vol 144, edited by W. S. D. Wilcock, E. F. Delong, D. S. Kelley, J. A. Baross, and S. C. Cary, pp. 245-268, AGU, Wahsington, D. C.

Von Damm, K. L. (2004), Evolution of the hydrothermal system at East Pacific Rise 9°50'N: Geochemical evidence for changes in the upper oceanic crust, in *Mid-Ocean Ridges: Hydrothermal Interactions Between the Lithosphere and Oceans, Geophys. Monogr. Ser.,* vol 148, edited by C. R. German, J. Lin, and L. M. Parson, pp. 285-304, AGU, Washington, D. C.

Welhan JA. (1988), Origins of methane in hydrothermal systems, *Chem. Geol*. 71:183-98.

Wilcock, W. S. D. (1998), Cellular convection models of mid-ocean ridge hydrothermal convection and the temperatures of black smoker fluids, *J. Geophys. Res., 103*, 2585-2596.

Wilcock, W. S. D., E. F. Delong, D. S. Kelley, J. A. Baross, and S. C. Cary, editors, (2004), The subseafloor biosphere at mid-ocean ridges, *Geophys. Monogr. Ser., v. 144,* 399 pp., American Geophys. Union, Washington, D. C.

William, D. L., and R. P. Von Herzen (1974), Heat loss from the Earth: New estimate, *Geology, 2*, 327-328.

Zoback, M. D., and R.N. Anderson (1983), Permeability, underpressures, and convection in the oceanic crust at Deep Sea Drilling Project Hole 504B. *In* Cann, J. R., Langseth, M. G., Honnorez, J., Von Herzen, R. P., White, S. M., et al., *Init. Repts. DSDP,* 69: Washington (U.S. Govt. Printing Office), 245-254.

Zyvoloski, G. A., Z. V. Dash, and S. Kelkar (1998), FEHM: Finite element heat and mass transfer code, *Rep. LA-11224-MS,* Los Alamos, Natl. Lab., Los Alamos, N. M.

Zyvoloski, G. A., B. A. Robinson, Z. D. Dash, and L. L. Trease (1997), Summary of models and methods for the FEHM application—A finite-element heat- and mass-transfer code, *Rep. LA-13307-MS,* Los Alamos, Natl. Lab., Los Alamos, N. M.